5. Temperature distribution inside the cask

In this chapter, stationary temperature situations under normal operation and non stationary temperature situations expected in case of fire are calculated for the TN 7-2 cask. Non stationary thermal calculations are carried out using the HEATING 5 program /5-1/.

5.1 Generalities

The cask is designed in such a way that it assures tight enclosure of the contents under the most different conditions. Heat is removed over the surface of the cask by natural convection and released to the environment.

Maximum decay heat released by the loaded fuel assemblies is found in chapter 2.3

Calculation of stationary temperature distribution is carried out separately for the different types of load. Non stationary heat calculations in an accidental fire are based on a representative model which covers all individual cases.

5.2 Stationary temperature distribution inside the cask

Calculations were carried out similarly to /5-2/ and /5-3/.

5.2.1 Calculation model

Temperature calculations are carried out for the horizontal central plane of the cask. The model is based on the following assumptions and simplifications:

1. The cask lies horizontally.
2. Transport is carried out dry.
3. Calculations are carried out in one dimension.
4. For calculation of the cask wall temperatures, heat sources inside the cask cavity are homogenised.
5. Gaps which may occur between the lead shielding and the surrounding layers disappear under operating conditions due to thermal expansion.
6. Thermal transfer from the exterior cask mantle occurs through convection and radiant heat transfer.

5.2.2 Initial data

5.2.2.1 Thermal powers

Thermal powers are also shown in chapter 2.3

A. DIDO and MERLIN fuel assemblies

Maximum thermal power per insert basket is 1125 W. There are four insert baskets in the cask. Maximum thermal power within the cask is 4500 W.

B. RHF fuel assemblies

Thermal power per fuel assembly: 2250 W at the utmost.
Maximum thermal power within the cask is 4500 W.

5.2.2.2 Geometry

Radial cask geometry in the central plane is shown in Fig. 5-1. Geometry of the insert baskets may be taken from the corresponding drawings.

5.2.2.3 Compilation of initial data

Table 5-1: Compilation of initial data for the assessment of cask body temperature

Index (Place)	Position	Material	Interior diameter [m]	$\alpha\left[\frac{W}{m^2K}\right]$	$\lambda\left[\frac{W}{m\,K}\right]$	ε[-]
∞	environment	air	-	-	0.0189	-
W	surface	steel/paint	1.03	3.66	-	0.9
1	exterior cladding	steel/paint	0.98	-	15	-
2	insulation	cement	0.938	-	1.6	-
3	shielding	lead	0.563	-	35	-
4	interior cladding	steel	0.54	-	15	0.55

5.2.3 Calculation of temperature distributions

A. DIDO and MERLIN fuel assemblies

The results of calculations are listed in table 5-3. Calculations are carried out according to the VDI-heat distribution chart /5-4/:

a) Temperature t_w at the surface of the cask

$$\dot{Q} = \varepsilon \cdot C_S \cdot A \cdot \left[\left(\frac{T_w}{100}\right)^4 - \left(\frac{T_\infty}{100}\right)^4\right] + \alpha_K \cdot A \cdot (t_w - t_\infty)$$

where ε = 0.90 (radiation coefficient of paint)

C_S = 5.77 (Stefan-Boltzmann constant)

A = 9.16 m^2 (total heat releasing surface between the two shock absorbers)

T_W = wall temperature in K

T_∞ = ambient temperature in K = 311 K (according to /5-5/)

α_K = hat transfer coefficient for a horizontal cylinder = f(Nu, Gr, Pr, λ)

$$Gr = \frac{g \cdot h \cdot l'^2 \cdot \beta \cdot (t_w - t_\infty)}{\nu^2} = 9{,}84 \cdot 10^9$$

$$l' = \frac{\pi}{2} \cdot d_a = 1{,}62 \text{ m}$$

$$h = d_a$$

Pr, β and ν related to t_m = 60 °C

$$Gr \cdot Pr = 9{,}84 \cdot 10^9 \cdot 0{,}69 = 6{,}79 \cdot 10^9$$

according to Fig. 1, Fa2 /5-4/, central curve according to Krischer:

$$Nu_{l'} = 205$$

$$\alpha_K = \frac{Nu_{l'} \cdot \lambda_m}{l'} = 3{,}66 \frac{W}{m^2 K}$$

t_w, t_∞ = temperatures in °C

Surface temperature t_W = 82 °C

Thus, surface temperature remains below the admissible limit according to /5-5/.

b) Temperature at cask surface with solar irradiation t_1

According to /5-5/, thermal flow due to solar irradiation over 24 h on the effective cask surface is:

$\emptyset$ = 193.5 W/m^2

This yields the following thermal power:

$$\dot{Q}_S = A \cdot \varepsilon \cdot \emptyset = 9{,}16 \cdot 0{,}3 \cdot 193{,}5$$

$$= 531{,}8 \text{ W}$$

Temperature t_1 is now calculated as follows:

$$t_1 = t_\infty + \frac{\dot{Q} + \dot{Q}_S}{\dot{Q}} \cdot (t_W - t_\infty)$$

$$= 38 + \frac{4500 + 531{,}8}{4500} \cdot (82 - 38)$$

$$= 88°C$$

c) Heat penetration through the basic body - temperature of interior cask wall t_4

$$\Delta t = \frac{\dot{Q}}{2\pi \cdot l} \cdot \left(\frac{\ln \frac{d_W}{d_1}}{\lambda_1} + \frac{\ln \frac{d_1}{d_2}}{\lambda_2} + \frac{\ln \frac{d_2}{d_3}}{\lambda_3} + \frac{\ln \frac{d_3}{d_4}}{\lambda_4}\right)$$

where: Δt = temperature gradient in cask wall

l = average length = $\frac{l_a + l_i}{2}$ = 2,84 m

Q = 4500 W

Further values are found in table 5-1.

$\Delta t = 12.1$ °C

$t_4 = t_1 + \Delta t = 99$ °C

Maximum temperatures of:

- cement : $t_2 = 94$ °C

- lead: $t_3 = 98$ °C

Thus temperatures of these materials remain below the admissible limits.

d) Temperature of insert basket and fuel assemblies

Calculations are carried out as in /5-2/. It is shown in /5-2/ that the highest temperatures occur in the DIDO insert basket; temperature distribution is thus calculated for this case. Calculations are carried out according to the following procedure:

1. Heat transfer from the exterior surface of the insert basket to the interior lining of the cask occurs through radiation. The surface of the interior lining is considered as heat transfer surface.

2. Residual heat of the four interior tubes plus 50 % of the heat of the exterior row of tubes is transferred from the walls of the exterior tubes to 1/3 of the perimeter.

3. The four central tubes transfer their heat to the exterior row of tubes through radiation.

$\dot{Q}$/ insert basket = 1125

$l_{basket} = 630$ mm

Only radiation is considered for the heat transfer from the cask wall to the exterior row of insert basket tubes (this is conservative). Exterior temperature of the exterior row of tubes is:

$$T_5^4 = T_4^4 + \frac{\dot{Q} \cdot 10^8}{\varepsilon \cdot A \cdot C_S}$$

where: T_4 = 372.6 K (temperature of the interior cask wall)

$\dot{Q}$ = 1125 W

ε = 0.55 (radiation coefficient of stainless steel)

$A = d \cdot \pi \cdot l = 0.54 \cdot \pi \cdot 0.63 = 1\text{-}07\ m^2$

(interior lining surface over the length of the basket)

C_S = 5.77

t_5 = 206 °C

Heat transfer in the exterior row of tubes due to conduction:

$$t_6 - t_5 = \frac{Q \cdot S}{\lambda \cdot A}$$

where: Q = 712/14 = 51 W

s = tube perimeter = $1/3 \cdot d \cdot \pi$ =

$1/3 \cdot 0.108 \cdot \pi = 0.11$ m

$A = 2 \cdot 0.005 \cdot 0.63 = 0.0063\ m^2$

λ = 15 W/mK

Temperature t_6 of the side of the exterior row of tubes facing the centre of the basket is:

t_6 = 265 °C

The four central tubes radiate onto the exterior row of tubes. Temperature t_7 of the side of the central tubes facing the exterior row of tubes is:

$$T_7^4 = T_6^4 + \frac{\dot{Q} \cdot 10^8}{\varepsilon \cdot A \cdot C_S}$$

$$= 8{,}377 \cdot 10^{10} + \frac{75 \cdot 10^8}{0{,}55 \cdot 0{,}068 \cdot 5{,}77}$$

$$t_7 = 314°C$$

Thermal conductivity through the wall of the central tube. Temperature t_8 of the interior wall:

$$t_8 - t_7 = \frac{Q \cdot S}{\lambda \cdot F} = \frac{75 \cdot 0{,}11}{2 \cdot 15 \cdot 0{,}0063}$$

$$t_8 = 358°C$$

Average temperature t_9 of the central basket tube:

$$t_9 = \frac{314 + 358}{2} = 336°C$$

Further calculation of fuel assembly temperature is carried out on the base of this average temperature.

Maximum fuel assembly temperature:

The fuel assemblies, which consist of 4 concentric cylinders, stand in the insert basket tubes. Thermal transfer between the single cylinders and the insert basket is due to radiation and conductivity in air. The following is valid:

$$Q = \varepsilon \cdot C_S \cdot A \cdot \left[\left(\frac{T_{10}}{100}\right)^4 - \left(\frac{T_9}{100}\right)^4\right] + A \cdot \frac{\lambda}{S} (t_{10} - t_9)$$

This allows to calculate temperatures up to the innermost fuel assembly cylinder temperature t_{13}. This is done on the base of following data:

Table 5-2: Input data to assess temperatures in the central fuel assemblies

Position	Thermal power Q (W)	Transmitting surface A (m^2)	Radiation number ε (-)	Thermal conduct. λ (W/mK)	Gap width S (m)
10/9	75	0.184	0.33	0.053	$2.4 \cdot 10^{-3}$
11/10	52	0.165	0.11	0.053	$3.4 \cdot 10^{-3}$
12/11	32	0.145	0.11	0.053	$3.4 \cdot 10^{-3}$
13/12	15	0.126	0.11	0.053	$3.4 \cdot 10^{-3}$

This yields the following results:

t_{10} = 351 °C

t_{11} = 370 °C

t_{12} = 383 °C

t_{13} = 390 °C

Temperature of a fuel assembly in an exterior row insert basket tube (Q = 125 W)

Exterior tube temperature: t_5 = 206 °C

Interior tube temperature: t_6 = 296 °C

Average temperature: t_m = 251 °C

The same pattern of calculation yields a temperature of less than 390 °C for the innermost fuel cylinder.

Table 5-3: Temperature distribution in a TN 7-2 cask loaded with DIDO and MERLIN fuel assemblies

Position		Temperature °C
Exterior cask wall		
- without solar irradiation	t_w	82
- with solar irradiation	t_1	88
Interior cask wall	t_4	100
Central insert basket	t_8	358
Interior fuel cylinder	t_{13}	390

The results show that temperature distribution within the cask has no influence on the tight enclosure. Temperatures remain below the admissible values for the different materials.

B. RHF fuel assemblies

The main results of calculations are listed in table 5-4.

As the thermal power in the cask is the same (Q = 4500 W) and it may be surmised that the heat releasing cask surface is identical, the following values may be taken over from 5.2.3.A, a) and b):

t_w = 82 °C
t_1 = 88 °C

Further calculations are carried out similarly to /5-3/.

c) Heat transfer through the basic body - interior cask wall temperature t_4

Assumption: heat propagates trapezoidally between the interior heat releasing length (l_i = 1.9 m) and the exterior heat releasing length (l = 2.53 m). The average diameter of the four cask layers is calculated according to:

$$d_m = \frac{d_a - d_i}{\ln \frac{d_a}{d_i}}$$

The length l_m obtained from this diameter is used to assess Δt.

Temperature differences are assessed according to:

$$t = \frac{\dot{Q}}{2 \cdot \pi \cdot l_m} \cdot \frac{\ln \frac{d_a}{d_i}}{\lambda}$$

where: $\dot{Q}$ = 4500 W

l_{m1} = 2.50 m

l_{m2} = 2.44 m

l_{m3} = 2.15 m

l_{m4} = 1.91 m

Further input data can be taken over from table 5-1.

$t_4 = t_1 + \Delta t$

$= 88 + (1.0 + 8.0 + 4.9 + 1.0)$

$= 103$ °C

t_2 = 97 °C (maximum temperature of cement)

t_3 = 102 °C (maximum temperature of lead)

No inadmissible material temperatures occur.

d) Temperature of fuel assembly t_6, t_7 and of insert basket t_5

Thermal transfer from the exterior cylinder of the RHF fuel assembly and the cask wall occurs through radiation and convection. Calculation is carried out according to equation:

$$Q = \varepsilon \cdot A_m \cdot C_{12} \cdot \left[\left(\frac{T_5}{100}\right)^4 - \left(\frac{T_4}{100}\right)^4\right] + \alpha_K \cdot A_m \cdot (t_5 - t_4)$$

with following initial data:

$$A_m = \left(\frac{d_a + d_i}{2}\right) \cdot \pi \cdot l_m$$

d_a = 0,54 m

d_i = 0,414 m

l_m = 1,98 m

ε_a = 0,55

ε_i = 0,11

$\dot{Q}$ = 4500 W

t_a = 103°C

α_{LK} = f (Pr,Gr,Nu,λ)

The obtained result is:

t_6 = 335 °C

The temperature of the interior fuel assembly tube is calculated assuming that half the heat of the assembly is transferred to the interior over the 280 fuel/aluminum plates. Due to the high aluminum contents and to the good thermal conductivity of aluminum, temperature gradient is small.

The following applies:

$$\Delta t = \frac{Q \cdot S}{\lambda \cdot A}$$

$Q = 2250/2 = 1125$ W

$$S = \frac{(d_a - d_i)}{2} = \frac{(0{,}41 - 0{,}26)}{2} = 0{,}075 \text{ m}$$

$\lambda = 100$ W/mK (assumed thermal conductivity of the fuel/aluminum plates)

$A = b \cdot l \cdot 280 = 0{,}00127 \cdot 0{,}9 \cdot 280 = 0{,}32$ m²

$$\Delta t = \frac{1125 \cdot 0{,}075}{100 \cdot 0{,}32} = 2{,}7°C$$

The temperature of the interior fuel assembly tube is:

$t_7 = 338$ °C

The temperature of the insert basket t_5 is lower than that of the fuel assembly.

The solidity of all materials is sufficient for the calculated temperatures.

Table 5-4: Temperature distribution in a TN 7-2 cask loaded with 2 RHF fuel assemblies.

Position		Temperature °C
Exterior cask wall		
- without solar irradiation	t_w	82
- with solar irradiation	t_1	88
Interior cask wall	t_4	103
Insert basket	t_5	< 338
Fuel assembly	t_7	338

5.3 Temperature distribution in the cask under accidental conditions

In accordance with IAEA regulations /5-5/, the cask will have to withstand half-hour accidental fires with a constant temperature of 800 °C. It will be demonstrated by way of non stationary calculation that even in case of an accidental fire, the admissible maximum temperature of the individual types of material will not be reached.

5.3.1 Description of the calculating program

The non stationary temperature calculation is carried out by two dimensional temperature calculation using the HEATING 5 program /5-1/.

This program is capable of solving the surface-heat-transfer equations in Cartesian and cylindrical co-ordinates (one-, two- and three-dimensional). An implicit difference method is applied for this.

The general formulation of the program allows for the processing of temperature- and location-dependent material data, apart from a large variety of other boundary conditions (radiation, convection, etc.)

5.3.2 Calculation model.

The model equivalent for temperature behaviour shown in Fig. 5-2 was compiled based on the geometry of the TN 7-2 transport cask according to drawing no. 1-150-050-04-00.

The model is based on following assumptions and simplifications:

1. The cask is lying horizontally.
2. Transport is carried out under dry conditions.
3. The calculation is carried out two-dimensionally.

4. The inside of the cask is homogenised. Conservatively, its heat capacity is taken into account. The heat source inside the cask is assumed so as to be representative for the different types of loading.

5. The shock absorbers are considered to be a homogeneous area. Deformations caused by a previous fall from a height of 9 m are taken into account with regard to the lid shock absorber.

6. Heat-surface-transfer on the outside of the cask takes place by convection and radiation.

7. The trunnions and the base plates are not taken into account in the calculation model.

8. Possible gaps within the cask body will disappear due to thermal expansion of the material.

9. Heat source density in the axial direction is assumed to be constant.

10. The heat-surface-transfer in the gap between the heat source and the inner lining is due to heat conduction and radiation.

11. It is conservatively assumed that the thermal conductivity of the cement will not decrease due to desiccation of the material during a fire. Evaporation heat required by evaporation of the water component of the cement is not taken into account. Two calculation runs are carried out as it is possible that the cement will not dry out completely, contrary to cask philosophy, and that thermal conductivity will thus decrease. The two runs will differ only by the thermal conductivity of the cement during the cooling phase.

    Run 1: λ_{cement} = 1.6 W/mK
    Run 2: λ_{cement} = 0.25 W/mK

5.3.3 Initial data and characteristic material data

5.3.3.1 Heat sources

The non stationary temperature calculation should be as general as possible in order to cover all considered types of loading. The following is assumed in order to assure this:

- The heat source inside the cask is homogenised. The dimensions of the cylindrical heat source are being assumed as follows:

- diameter: 0.473 m
- height: 2.5 m
- distance from
the cask bottom: 0.1 m
- distance from
the cask lid: 0.07 m

The gap between the inner cask wall with a diameter of 0.54 m and the heat source is being chosen at a conservatively high value so that little heat will be transferred into the cask inside.

- The thermal power of the load is 4.5 kW.
- The heat source was conservatively not assigned any thermal capacity.

5.3.3.2 Characteristic material data

The individual material data have been derived from the literature or manufacturer's information. Fig. 5-2 shows the various types of materials used for the calculation model.

Material 1: stainless steel

$$\lambda = 15 \frac{W}{mk}$$

$$\rho = 7880 \frac{kg}{m^3}$$

$$C_p = 500 \frac{J}{kgK}$$

Material 2: lead

$$\lambda = 35 \frac{W}{mk}$$

$$\rho = 11200 \frac{kg}{m^3}$$

$$C_p = 130 \frac{J}{kgK}$$

Material 3: thermal insulation (cement)

$$\lambda = 1.6 \frac{W}{mk} \quad \text{(hydrated cement)}$$

$$\lambda = 0.25 \frac{W}{mk} \quad \text{(dehydrated cement)}$$

$$\rho = 1890 \frac{kg}{m^3}$$

$$C_p = 3150 \frac{J}{kgK}$$

Desiccation of the cement starts at 100 °C and is completed at approximately 200 °C. For the purpose of calculation it is conservatively assumed that the heat conductivity and the specific thermal capacity do not change between these temperature values (i.e. λ is assumed to remain constant at 1.6 W/mK during a fire).

Material 4: shock absorbers

The shock absorbers consist of balsa wood as well as of a metal sheet casing and steel rods. An effective value for λ is determined higher than the heat conductivity of balsa wood.

$$\lambda = 0.1 \frac{W}{mk}$$

$$\rho = 135 \frac{kg}{m^3}$$

$$C_p = 2721 \frac{J}{kgK}$$

Material 5:

Material 5 is the homogenised area of insert basket components and fuel assemblies. The effective material values are conservatively estimated:

$$\lambda_{eff} = 4 \frac{W}{mk}$$

$$\rho_{eff} = 1460 \frac{kg}{m^3}$$

$$C_{p\ eff} = 10 \frac{J}{kgK}$$

The thermal capacity of the homogenised inside area is conservatively set to 0.

Material 6: air

Temperature dependence of the heat conductivity of air is taken into account. The values quoted in 20 °C steps in /5-4/ are interpolated linearly and C_p is assumed to be constant.

$$\rho = 1 \frac{kg}{m^3}$$

$$C_p = 1000 \frac{J}{kgK}$$

5.3.3.3 Thermal transitions

- The thermal transition between a fire and the cask body is assured by radiation and convection.

According to /5-7/, the thermal radiation transition coefficient α_S is 90 % for a flame temperature of approximately 800 °C and the natural convection coefficient α_K is 10 % of the total thermal transition coefficient α_{Ges}.

The emission coefficient of flames is $\varepsilon_F = 0.7 - 0.9$ according to literature. For calculations, $\varepsilon_F = 1$ is assumed (conservatively).

The absorption coefficient ε of the surface is also set to 1 in order to take account of a change in the coefficient due to sooting.

The amount of heat assumed per unit area is determined by:

$$q'' = \alpha_K \cdot (T_F - T_0) + \alpha_S \cdot (T_F - T_0) \ \frac{W}{m^2}$$

where $$\alpha_S = \varepsilon \cdot \sigma \cdot (T_F^2 + T_0^2)\ (T_F - T_0)$$

$$\alpha_K = \frac{0,1}{0,9} \cdot \alpha_S = 0,11\ \alpha_S$$

$$q'' = \varepsilon \cdot 1,1 \cdot \sigma \cdot (T_F^4 - T_0^4) =$$

$$= 6,34 \cdot 10^{-8} \cdot (T_F^4 - T_0^4)\ \frac{W}{m^2}$$

- During the cooling stage thermal transition to the environment takes place by radiation and convection over the cask mantle and the mantle and ends of the shock absorbers.

1. Radiation

$$\dot{q} = \bar{\varepsilon} \cdot (T_i^4 - T_a^4)$$

ε = 0.9 (radiation coefficient of the paint layers)

σ = Stefan-Boltzmann constant

$$\bar{\varepsilon} = \varepsilon \cdot \sigma = 0.9 \cdot 5.77 \cdot 10^{-8}$$

$$= 5.2 \cdot 10^{-8} \frac{W}{m^2 K^4}$$

2. Convection

$$\dot{q} = \alpha_K \cdot (T_i - T_a)\ W/m^2$$

The thermal transition factor α_K is a function of the Grasshoff, Prandl and Nusselt numbers and of the heat conductivity λ.

$$\alpha_K = f(Gr, Pr, Nu, \lambda)$$

The Grasshoff number is derived from:

Nu = f (Gr, Pr) according to the average curve of 0.
Krischer, from /5-4/.

and α_K from:

$$\alpha_K = \frac{Nu \cdot \lambda}{\frac{\pi}{2} \cdot D} \qquad \text{(mantle parts)}$$

$$\alpha_K = \frac{Nu \cdot \lambda}{D/2} \qquad \text{(front end)}$$

- Thermal transition in the gap between the inner cask wall and the homogenised insert basket and fuel assembly area takes place by radiation and conduction.

  The radiation coefficient for stainless steel is assumed to be $\varepsilon_a = 0.55$, the radiation coefficient for the homogenised source area to be $\varepsilon = 0.55$.

5.3.4 Results of non stationary thermal calculations

The results of the non stationary calculations for the instants t = 0 s (start of the fire), 1,800 s (end of the fire) and 12,600 s (end of calculations) are found in the computer printouts, Tables 5-5, 5-6 and 5-7.

Table 5-8 and fig. 5-3 show the time dependence of temperature for several key locations on the cask.

- During the fire, the temperature of the outer steel wall rises to a maximum of 642 °C at the centre of the cask and decreases again rapidly.

- The maximum temperature of lead, 285 °C, is reached during the cooling phase at t = 4,800 s. There will thus be melting of lead.

- The maximum gasket temperature of 177.5 °C occurs during the cooling stage at the end of calculations, at t = 12,600 s. At this point in time a slight increase in the gasket temperature can still be observed. The increase is, however, so slight that a temperature of less than 185 °C may be expected. The proper functioning of the gaskets will not be impaired.

- The temperature of the inner cask wall will reach a maximum of 286 °C at t = 4,800 s.

A second calculation run will be carried out in addition to the first, with preliminary requirements changed in one respect. The heat conductivity of cement was no longer assumed to be constant at 1.6 W/mK, but a heat conductivity of the dehydrated cement of 0.25 W/mK was assumed for the cooling stage.

The results of this calculation run correspond to those of the preceding run until t = 1,800 s (see Tables 5-5, 5-6). The results for t = 14,000 s (end of calculations) are listed in Table 5-9. Table 5-10 and Fig. 5-4 show the time dependence of the temperature for several key points. It should be noted that under these conditions, which are obviously conservative, the corresponding temperatures are lower than or approximately equal to those observed during the first calculation run. The following maximum temperatures are obtained:

- cask surface: 641,6 °C
- lead shielding: 244,5 °C
- lid gasket: 169,6 °C
- inner cask wall: 244,5 °C

It should be noted here that the gasket temperatures reached their maximum value at the end of calculations and that a slight increase in temperature could be observed at that time. It may, however, be assumed that the temperature of less than 185 °C calculated during the first run will not be exceeded. The higher temperature of the inner wall determined during the first run is used as a base for calculating the temperature of the insert basket and of fuel assemblies during a fire.

HEATINGS

TRANSIENT TEMPERATURE DISTRIBUTION AFTER 0 TIME STEPS, TIME = 0.

GROSS GRID		1										
FINE GRID		1	2	3	4	5	6	7	8	9	10	11
DISTANCE		.03	.12	.24	.27	.28	.30	.40	.47	.49	.52	.83
1	1	0.00	39.67	39.65	39.62	39.60	39.59	39.58	39.49	39.39	39.36	39.31	38.05
	2	.19	63.13	62.92	62.66	61.98	61.89	61.89	60.38	58.88	58.33	57.55	38.68
	3	.37	88.67	88.19	87.31	87.03	86.95	86.79	86.08	84.91	84.61	84.26	39.48
	4	.90	88.75	88.36	87.34	87.06	86.98	86.82	86.15	84.94	84.62	84.51	39.51
	5	.97	89.17	88.71	87.50	87.15	87.05	86.86	86.13	85.83	84.52	84.43	39.51
	6	.97	90.73	90.14	85.09	87.32	87.14	86.87	85.91	85.39	83.15	82.98	39.40
	7	.98	91.71	91.01	88.61	87.10	86.99	86.85	85.88	85.31	82.64	82.43	39.33
	8	.68	272.03	266.30	249.70	87.35	87.27	87.09	85.66	84.57	77.12	75.67	38.44
	9	.69	287.20	281.00	262.90	87.99	87.52	87.16	85.66	84.55	77.32	76.43	0.00
	10	1.00	322.80	314.80	290.40	91.46	90.82	90.31	88.23	87.08	80.69	79.88	0.00
	11	1.31	334.01	325.30	299.20	93.74	93.06	92.51	90.29	89.09	82.43	81.58	0.00
	12	1.63	337.43	328.69	302.00	94.99	94.30	93.74	91.47	90.24	83.40	82.53	0.00
	13	1.94	336.21	329.11	301.60	95.35	94.66	94.10	91.83	90.59	83.69	82.82	0.00
	14	2.25	337.43	328.50	301.90	94.91	94.23	93.67	91.41	90.18	83.35	82.48	0.00
	15	2.56	333.93	325.20	299.10	93.61	92.93	92.39	90.18	88.98	82.33	81.49	0.00
	16	2.88	322.51	314.40	290.10	91.39	90.66	90.15	88.08	86.94	80.57	79.77	0.00
	17	3.19	286.19	279.93	261.00	87.85	87.41	87.04	85.48	84.38	77.29	76.42	0.00
	18	3.21	237.43	232.70	219.30	87.11	87.05	86.89	85.46	84.41	76.77	74.87	38.38
	19	3.26	91.47	90.61	88.35	87.17	86.95	86.69	85.47	84.71	80.77	80.40	39.14
	20	3.27	90.86	90.21	88.45	87.42	87.25	86.67	85.47	84.76	81.36	81.10	39.23
	21	3.38	89.07	88.54	87.46	87.12	87.02	86.60	85.58	85.00	84.49	84.33	39.48
	22	3.44	88.67	88.23	87.28	87.20	86.91	86.65	85.72	84.90	84.65	84.40	39.45
	23	3.51	88.31	88.01	87.11	86.83	86.74	86.57	85.80	76.87	75.07	73.20	39.19
	24	3.61	61.93	61.69	61.61	60.15	60.00	59.67	57.49	55.05	54.30	53.34	38.54
	25	3.76	39.41	39.41	39.35	39.32	39.31	39.29	39.16	39.03	38.98	38.93	38.04

Table 5-5: Temperature distribution at time t = 0 s
(Beginning of fire) First calculation run

HEATING5

TRANSIENT TEMPERATURE DISTRIBUTION AFTER 82 TIME STEPS, TIME = 1.80000E+03

GROSS GRID			1										
			1		3	4	5	6	7	8	9	10	11
FINE GRID		DISTANCE	.00	.12	.24	.27	.28	.30	.40	.47	.49	.52	.83
1	1	0.000	798.75	798.75	798.74	798.74	798.74	798.74	798.74	798.74	798.74	798.75	800.00
	2	.19	72.71	72.50	71.85	71.57	71.48	71.28	69.98	68.71	69.44	73.43	799.34
	3	.37	91.45	90.82	92.[illegible]	92.63	92.71	92.82	91.40	87.25	87.67	88.41	799.35
	4	.40	91.99	91.65	93.[illegible]	94.24	94.37	94.56	93.03	87.22	88.04	88.46	799.35
	5	.47	92.70	93.75	97.80	99.63	100.16	101.16	104.57	103.52	96.74	98.56	799.36
	6	.57	96.97	96.57	104.77	111.78	113.95	117.45	129.61	134.75	156.75	158.56	799.41
	7	.58	95.77	97.43	105.27	117.08	119.13	121.55	135.24	143.34	191.55	196.40	799.44
	8	.63	107.61	282.62	260.05	151.29	152.10	154.14	182.88	224.15	617.61	706.40	799.98
	9	.69	301.89	294.39	281.35	153.89	154.55	156.25	185.87	228.64	614.42	674.41	0.00
	10	1.00	344.54	337.03	314.23	169.05	169.57	171.64	200.44	237.88	579.80	641.13	0.00
	11	1.31	350.79	348.56	323.91	171.60	172.09	174.13	202.60	239.61	579.82	641.06	0.00
	12	1.63	360.40	351.98	326.20	172.79	173.27	175.30	203.68	240.62	580.30	641.43	0.00
	13	1.94	361.19	352.74	327.37	173.15	173.62	175.65	204.02	240.93	580.45	641.55	0.00
	14	2.25	360.34	351.93	326.71	172.74	173.21	175.24	203.63	240.57	580.27	641.41	0.00
	15	2.56	358.60	348.39	323.76	171.47	171.96	174.00	202.48	239.50	579.77	641.02	0.00
	16	2.88	344.04	336.52	313.[illegible]	166.56	169.07	171.13	199.91	237.39	579.53	640.91	0.00
	17	3.19	302.50	290.96	279.90	150.54	150.98	152.80	181.77	223.64	604.16	664.83	0.00
	18	3.21	250.82	247.17	237.99	144.62	145.47	147.58	174.68	212.54	603.23	714.65	799.99
	19	3.26	98.32	98.22	107.90	121.25	125.74	129.61	149.78	166.48	283.34	296.50	799.53
	20	3.27	95.69	97.66	107.[illegible]	114.71	116.97	126.34	145.62	159.27	240.25	246.80	799.48
	21	3.38	92.45	93.47	97.39	99.14	99.70	103.03	111.39	111.91	109.80	109.53	799.37
	22	3.44	90.67	91.12	9[illegible].[illegible]	92.66	92.53	92.33	95.76	98.99	98.10	96.15	799.36
	23	3.51	87.08	89.04	89.04	88.93	88.89	88.83	89.43	77.57	77.20	80.21	799.35
	24	3.61	90.41	92.10	91.13	90.72	90.58	90.26	88.21	85.85	86.34	90.04	799.36
	25	3.72	797.85	797.85	797.84	797.84	797.84	797.84	797.84	797.83	797.83	797.84	800.00

Table 5-6: Temperature distribution at time t = 1800 s (End of fire) First calculation run

HEATING5

TRANSIENT TEMPERATURE DISTRIBUTION AFTER 206 TIME STEPS, TIME = 1.26000E+04

GROSS GRID	FINE GRID	DISTANCE	1 .00	2 .12	3 .24	4 .27	5 .28	6 .30	7 .40	8 .47	9 .49	10 .52	11 .83
1	1	0.00	46.93	46.93	46.91	46.90	46.89	46.89	46.85	46.88	46.88	46.84	40.70
	2	.19	82.32	82.20	81.79	81.50	81.42	81.26	80.51	81.67	82.41	83.35	58.91
	3	.37	178.76	178.32	176.76	176.45	176.14	175.67	172.04	160.17	158.09	155.67	60.79
	4	.40	179.93	178.48	177.1[illegible]	176.92	176.32	175.88	172.82	160.22	158.52	157.90	60.87
	5	.47	179.61	179.15	177.[illegible]	177.44	177.19	176.89	175.22	173.40	165.21	164.62	60.89
	6	.57	181.59	181.03	179.[illegible]	178.97	178.89	178.73	177.05	175.54	167.48	166.89	59.14
	7	.58	182.62	182.08	180.[illegible]	179.25	179.24	179.14	177.39	175.78	166.54	165.79	57.88
	8	.68	324.37	314.70	296.[illegible]	193.92	183.31	183.34	180.10	176.87	150.59	145.04	41.25
	9	.69	333.07	325.96	307.[illegible]	194.42	183.91	183.46	180.40	177.11	151.77	148.36	0.00
	10	1.00	371.74	365.65	341.[illegible]	207.39	206.09	206.03	202.44	199.57	177.29	173.68	0.00
	11	1.31	390.31	381.67	355.[illegible]	224.09	223.34	222.63	218.66	215.46	190.18	186.08	0.00
	12	1.63	377.17	368.35	361.[illegible]	232.36	231.59	230.86	226.65	223.16	195.79	191.42	0.00
	13	1.94	393.03	390.16	363.[illegible]	234.64	233.87	233.13	228.85	225.25	197.22	192.79	0.00
	14	2.25	387.10	388.27	361.[illegible]	232.21	231.44	230.71	226.50	223.01	195.67	191.32	0.00
	15	2.56	390.19	381.54	355.[illegible]	224.82	224.07	222.35	218.39	215.19	189.94	185.84	0.00
	16	2.88	373.57	365.49	341.[illegible]	207.28	206.98	205.93	202.34	199.44	177.08	173.48	0.00
	17	3.19	341.63	325.58	306.[illegible]	185.38	184.88	184.43	181.47	178.23	153.23	149.86	0.00
	18	3.21	294.28	289.70	270.[illegible]	183.86	183.79	183.56	180.89	177.83	150.77	143.41	41.68
	19	3.26	187.74	182.43	181.[illegible]	181.43	181.53	181.40	179.58	177.65	165.13	163.92	54.85
	20	3.27	182.05	181.83	181.[illegible]	181.07	181.07	181.04	179.38	177.61	167.16	166.35	56.51
	21	3.38	177.55	179.45	179.[illegible]	179.02	178.99	178.89	177.95	176.75	175.33	174.90	60.84
	22	3.44	175.50	178.43	178.[illegible]	177.89	177.80	177.52	176.91	175.75	175.01	174.06	61.08
	23	3.51	176.88	176.88	176.[illegible]	176.52	176.45	176.30	175.50	122.34	115.74	111.55	60.01
	24	3.61	100.84	100.89	100.[illegible]	100.46	100.39	100.20	98.42	92.32	91.59	90.98	57.18
	25	3.72	44.73	44.73	44.[illegible]	44.69	44.68	44.66	44.50	44.10	44.05	44.01	40.43

Table 5-7: Temperature distribution at time t = 12600 s (3 h after end of fire) First calculation run

Table 5-8: Time dependence of temperature in °C at some points on the cask. First calculation run

Place Time (s)	Cask surface (central plane)	Lead shielding (exterior radius)	Lid gasket	Protective lid gasket at the bottom	Interior cask wall (central plane)
0	82,8	90,6	86,7	86,9	95,4
10	99,0	90,6	86,7	86,9	95,4
20	113,5	90,6	86,7	86,9	95,4
40	138,1	90,7	86,7	86,9	95,4
80	175,8	91,0	86,7	86,9	95,4
160	229,0	92,8	86,7	86,9	95,4
320	308,4	100,5	86,7	86,9	95,8
640	432,1	125,3	86,7	87,3	100,5
1280	582,0	188,7	88,3	92,4	132,0
1800	641,6	240,9	92,3	101,2	173,1
1840	594,4	244,8	92,8	102,0	176,6
1880	566,4	248,3	93,2	102,8	180,1
1960	532,3	254,4	94,1	104,6	187,2
2220	465,1	267,2	97,6	110,6	209,7
2500	413,4	274,3	102,0	117,3	230,2
2800	372,1	279,3	107,2	124,2	248,2
3400	317,1	283,2	117,9	136,4	270,4
4000	283,9	283,3	128,0	146,0	280,9
4800	257,5	280,2	139,5	155,7	285,1
5800	238,9	273,9	150,8	164,0	282,7
7000	225,8	265,0	160,6	170,2	275,3
8000	218,1	257,3	166,5	173,3	267,9
9500	208,8	246,2	172,3	175,9	256,5
11000	200,7	235,7	175,7	176,9	245,5
12600	192,8	225,3	177,5	176,9	234,6

Table 5-9: Temperature distribution at time t = 14000 s
(3 h and 23 min. after end of fire) Second calculation run

TN 7/2 Non stationary temperature distribution in a 800 °C fire and during cooling

HEATINGS

TRANSIENT TEMPERATURE DISTRIBUTION AFTER 84 TIME STEPS, TIME = 1.40000E+04

GROSS GRID			1									
	FINE GRID		1	2	3	4	5	6	7	8	9	10	11
	DISTANCE		.00	.12	.24	.27	.28	.30	.40	.47	.49	.52	.83
1	1	0.00	44.92	44.91	44.89	44.88	44.87	44.87	44.84	44.87	44.87	44.85	39.90
	2	.19	82.02	81.89	81.43	81.21	81.14	81.00	80.41	81.48	82.05	82.71	54.18
	3	.37	171.94	171.79	171.18	170.75	170.56	170.18	166.32	150.12	147.39	145.13	55.91
	4	.40	172.28	172.12	171.52	171.12	170.97	170.61	167.48	149.92	147.16	146.46	55.97
	5	.47	173.24	173.11	172.72	172.59	172.54	172.44	171.75	171.43	149.04	147.75	55.94
	6	.57	175.32	175.17	174.92	175.25	175.38	175.56	175.13	174.44	145.79	145.45	54.42
	7	.58	176.32	176.12	175.93	175.89	176.15	176.26	175.76	175.00	143.84	143.43	53.42
	8	.68	318.49	312.91	297.90	182.34	182.27	182.10	180.61	179.28	119.40	116.32	40.51
	9	.69	330.56	324.51	305.88	183.45	182.98	182.83	181.04	179.67	119.40	117.59	0.00
	10	1.00	372.58	364.51	340.20	205.98	205.33	204.78	202.42	200.97	137.65	135.57	0.00
	11	1.31	389.40	380.77	354.36	222.96	222.26	221.66	219.06	217.46	144.68	142.39	0.00
	12	1.63	396.63	387.84	361.48	232.38	231.66	231.06	228.33	226.59	147.45	145.05	0.00
	13	1.94	398.67	389.84	363.38	235.21	234.49	233.88	231.12	229.33	148.17	145.74	0.00
	14	2.25	396.50	387.71	361.36	232.16	231.45	230.84	228.12	226.38	147.39	144.99	0.00
	15	2.56	389.12	380.49	354.59	224.52	223.82	223.22	220.63	219.03	144.55	142.26	0.00
	16	2.88	372.05	363.97	339.72	205.32	204.67	204.13	201.78	200.35	137.61	135.54	0.00
	17	3.19	329.42	323.41	304.59	183.44	181.98	181.62	180.09	178.79	121.63	119.84	0.00
	18	3.21	290.67	286.20	273.65	180.52	180.48	180.36	179.08	177.85	122.25	117.92	40.85
	19	3.26	174.86	174.90	175.13	176.22	176.68	176.83	176.19	175.22	141.93	141.32	50.94
	20	3.27	174.16	174.25	174.70	175.31	175.50	176.21	175.70	174.74	145.01	144.60	52.22
	21	3.33	171.43	171.51	171.73	171.82	171.85	172.04	171.48	167.55	165.82	164.90	55.98
	22	3.44	170.13	170.20	170.23	170.02	169.91	169.61	169.21	167.50	166.27	165.06	56.20
	23	3.51	168.20	166.28	168.31	168.14	168.08	167.94	167.27	120.34	114.50	110.70	55.21
	24	3.61	99.10	99.04	98.87	98.67	98.60	98.42	96.74	91.14	90.31	89.47	52.73
	25	3.72	44.39	44.38	44.36	44.34	44.33	44.31	44.16	43.78	43.72	43.65	39.85

Table 5-10: Time dependence of temperature in °C at some points on the cask. Second calculation run

Place Time (s)	Cask surface (central plane)	Lead shielding (exterior radius)	Lid gasket	Protective lid gasket at the bottom	Interior cask wall (central plane)
1800	641,6	240,9	92,3	101,2	173,1
1850	588,3	236,1	92,9	102,2	177,4
2000	536,2	228,6	94,7	105,4	189,4
2500	459,9	224,9	101,5	115,1	211,9
3000	404,7	227,6	108,4	122,5	221,7
4000	328,7	238,4	120,4	133,5	232,2
5000	278,9	237,3	130,4	141,8	238,3
8000	199,5	240,2	151,3	158,0	244,5
10000	173,3	238,0	159,9	165,7	243,2
14000	145,7	229,3	169,6	172,4	235,2

5.3.5 Insert basket and fuel temperature during accidental fires

No non stationary calculations is carried out to determine the maximum temperature of the insert baskets and fuel assemblies. The temperature is calculated on the basis of the calculated maximum temperature of the interior wall during an accidental fire. Calculation is continued inwards in analogy to the determination of the temperature distribution under routine operating conditions (cf. also chapter 5.2).

The maximum temperature of the inner wall during an accidental fire is 286 °C.

A. DIDO and MERLIN fuel assemblies

Thermal calculations using the new initial temperature yield the temperature distribution shown below. Calculations are only carried out for DIDO fuel assemblies as higher temperatures are expected with them.

Table 5-11: Temperature distribution in the DIDO basket during an accidental fire

Position	Temperature °C
- Interior wall temperature t_4	286
- Temperature of exterior fuel shafts	
- exterior t_5	331
- interior t_6	390
- Temperature of the exterior wall of the central fuel shaft t_7	418
- Temperature of the interior wall of the central fuel shaft t_8	462
- Average temperature of the central fuel shaft t_9	440
- Temperature of the exterior fuel assembly tube t_{10}	452
- Temperature of the innermost fuel assembly tube t_{13}	479

The maximum temperature of the basket is approximately 462 °C.

Thus, sufficient solidity of the stainless steel can be guaranteed. The maximum temperature of the fuel assemblies is 479 °C, which is considerably lower than the melting point of the material of 600 °C.

B. RHF fuel assemblies

During an accidental fire the maximum temperature of a fuel assembly is t_7 = 440 °C, whilst temperature t_4 of the inner cask wall is 286 °C. The temperature limit of 600 °C will not be reached.

5.4 Fire test on a TN 7-2 1/3 scale model

Apart from the non stationary thermal calculations, a fire test was carried out with a 1/3 scale model of the TN 7-2 in order to investigate the behaviour of the cask in an accidental fire.

The fire test was used to determine the heating-up graph of the cask and to investigate the vapour pressure behaviour of the cement.

According to model laws, a heating up period of approximately 3.5 min would suffice. As an exact determination of the duration of a fire for the 1/3 scale model, which would be representative for the 30 minute fire exposure of a full size cask, is not possible, the test was stopped when the melting point of lead was reached. Effects which would occur on account of a fire lasting too long were not taken into consideration.

The locations of the measurement points can be found in the enclosed measurement location plan.

The test was carried out in a closed furnace of the Federal Institute for Materials Testing. It was heated by oil burners.

The burners were switched off after 9 minutes and 57 seconds. At this point the melting point of lead was reached.

The temperature development during and after the fire can be seen in the enclosed figure. It appears that heating over the perimeter of the cask model is irregular (cf. comparison of measurement locations 2 and 5).

In spite of the fact that the melting point of lead was exceeded at several locations on the cask, the temperatures measured at the gaskets remained considerably below the admissible values which have to be withstood for short periods of time by the gasket material without impairing its specific functions

No changes of the cask due to melting of lead and building up of pressure in the cement layer were found.

A detailed description of the test can be found in /5-8/.

5.5 Literature

/5-1/ Turner, Elrof, Siman-Tov
HEATING 5
Computer Sciences Division, Oak Ridge, Tennessee

/5-2/ TN 7-2/MTR Package Design, Safety Report
TN Report no. 7701

/5-3/ Safety Analysis Report, Transport of two Irradiated RHF Fuel Assemblies in the TN 7 Cask,
TN Report no. 8021

/5-4/ VDI-Wärmeatlas, 3rd Edition, 1977

/5-5/ IAEA Regulations for the Safe Transport of Radioactive Materials, 1973

/5-6/ C.W. Wegst, Steel Codes
Verlag Stahlschlüssel Wegst GmbH & Co., Marbach, 1980

/5-7/ S. Aoki, H. Shimada, K. Tamura
Assessments of the Heat Transfer Properties of Spent Fuel Shipping Casks (1976)

/5-8/ Instrumented Drop and Fire Tests on a Model Spent Fuel Transport Cask of the TN 7-2 Type,
Test Report no. 2041
Federal Institute for Materials Testing Berlin
May 19, 1982

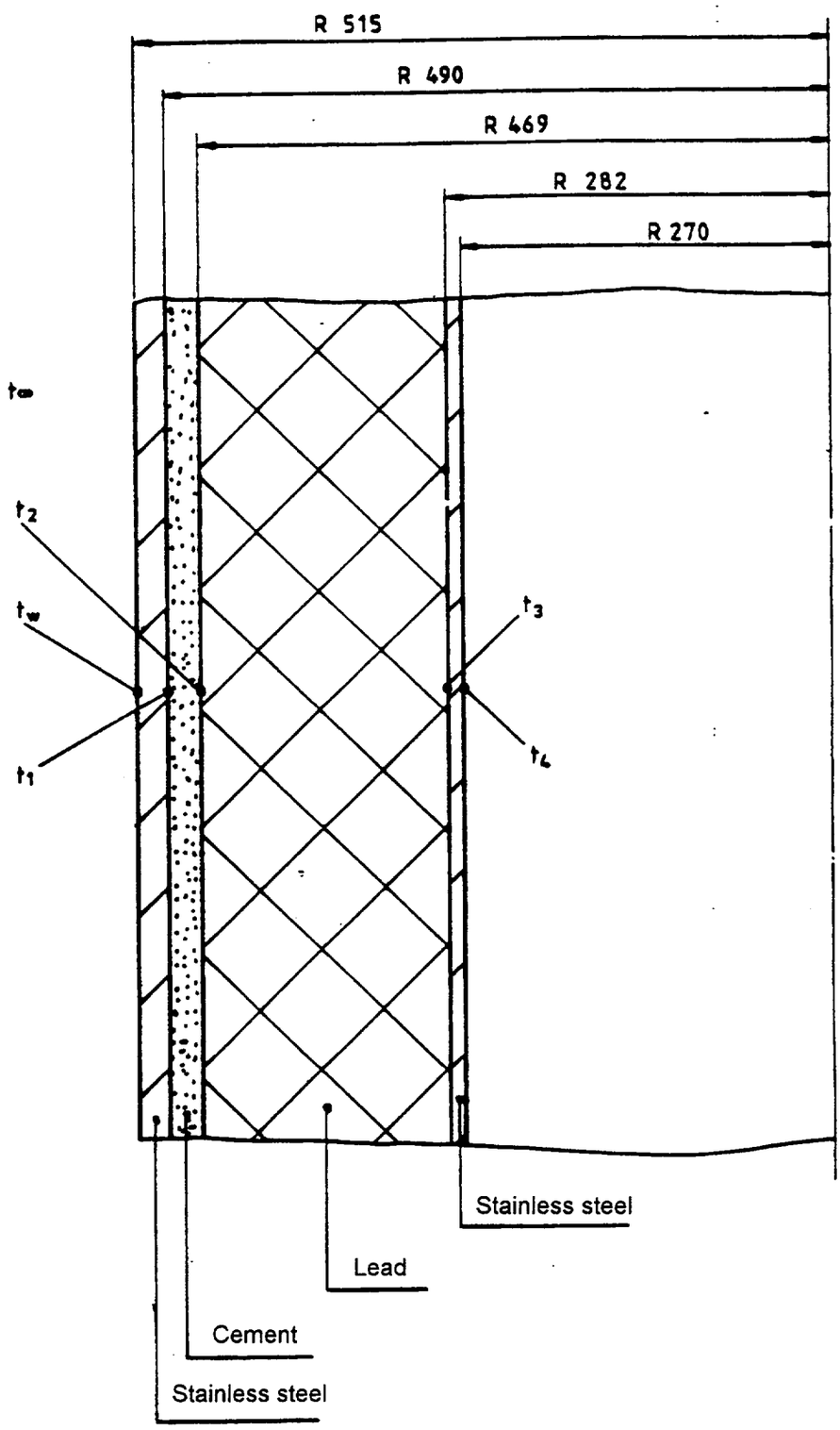

TN	Section throught the central plane of the cask	Fig. 5-1

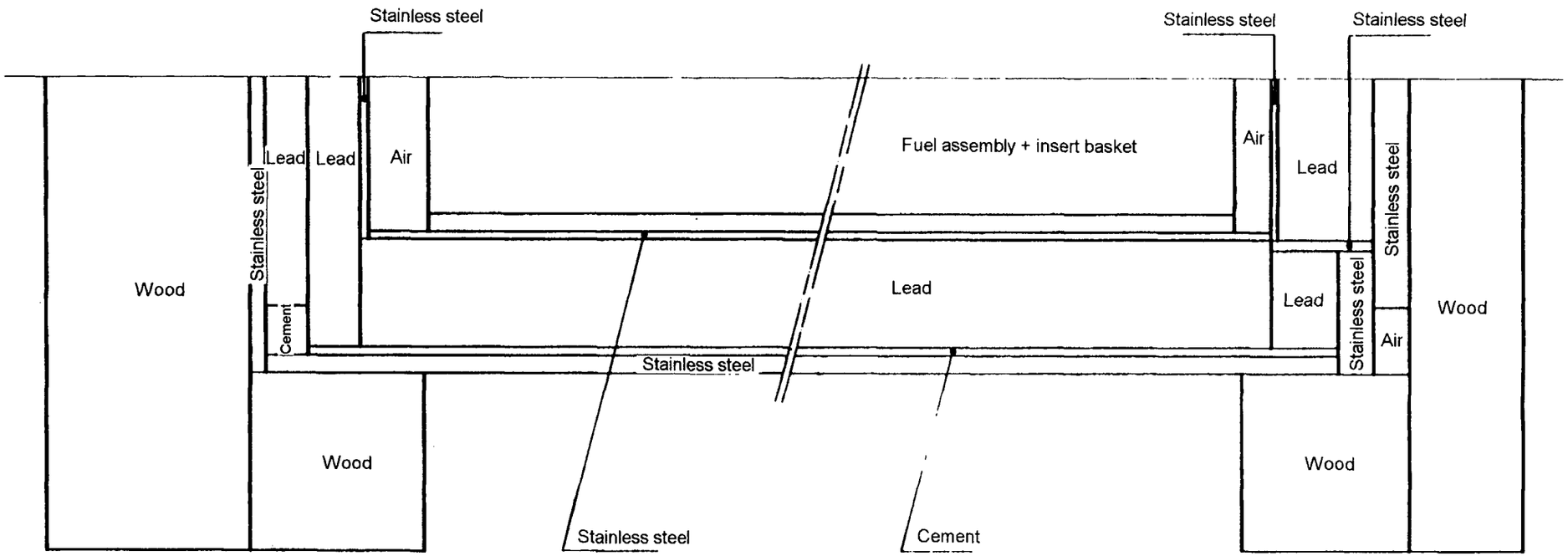

Bottom end

Lid end

TN	Calculation model of the TN 7-2 for non stationary thermal calculation	Fig. 5-2

Calculation run 1

Fire phase: λ_{cement} = 1.6 W/mk

Cooling phase: λ_{cement} = 1.6 W/mk

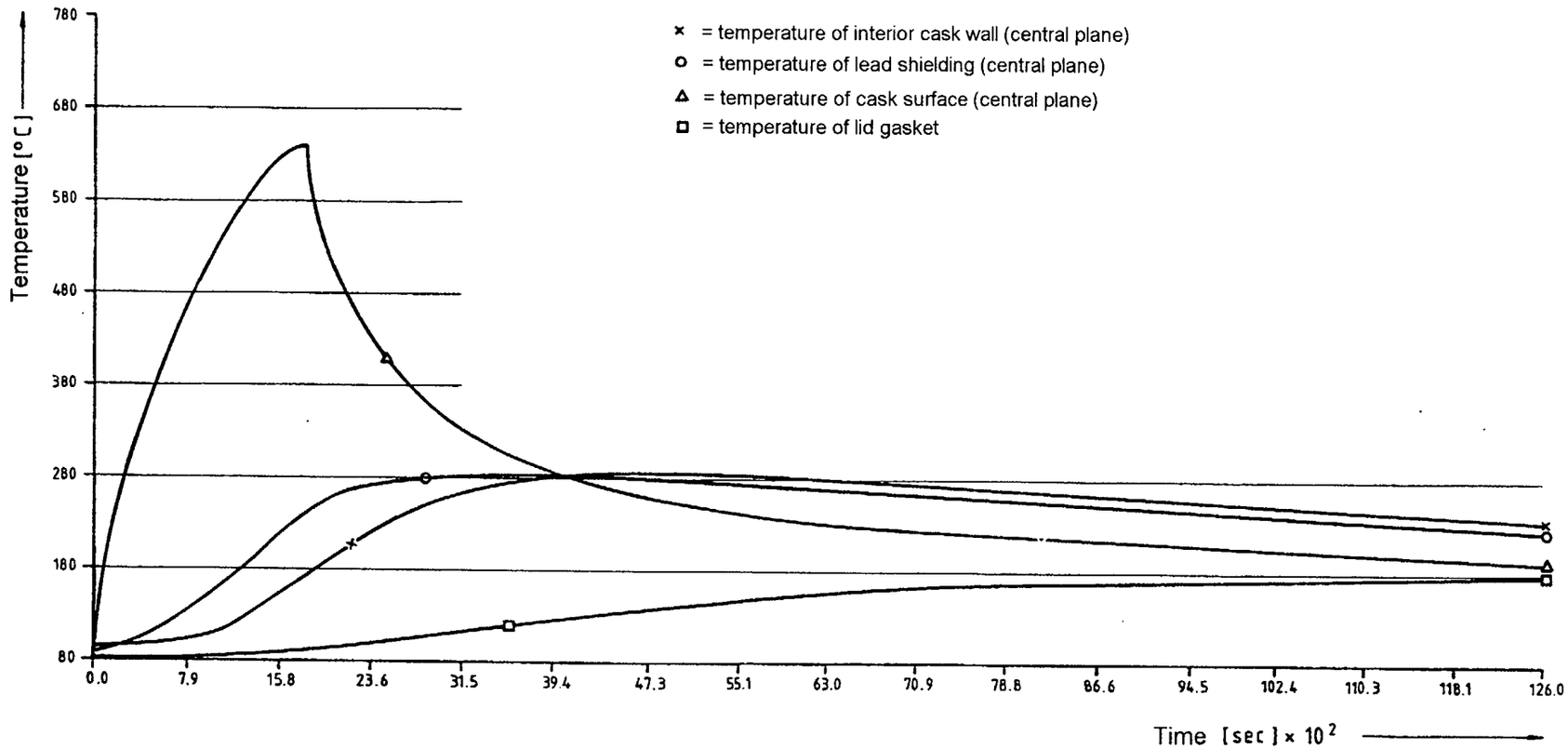

TN	Time dependence of temperature for the TN 7-2 cask in an accidental fire	Fig. 5-3

Calculation run 2

Fire phase: λ_{cement} = 1.6 W/mk

Cooling phase: λ_{cement} = 0.25 W/mk

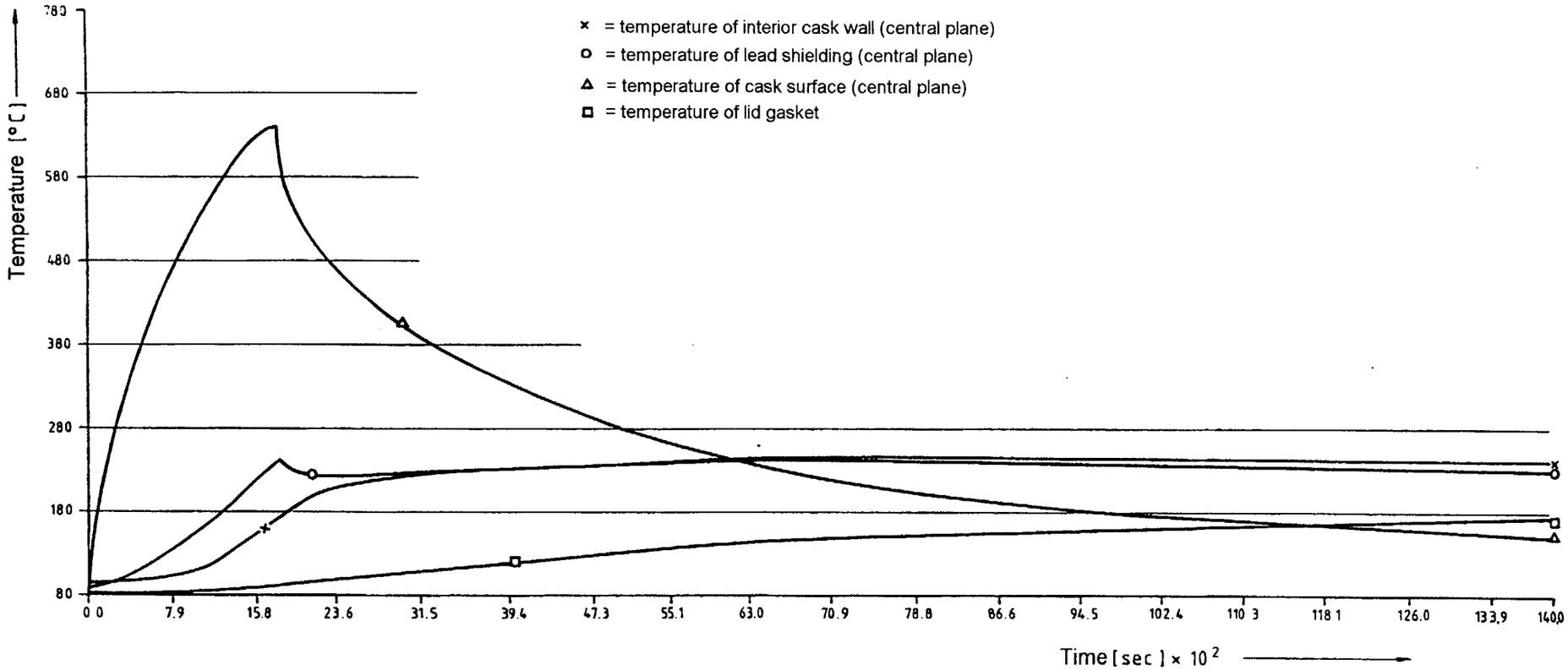

TN	Time dependence of temperature for the TN 7-2 cask in an accidental fire	Fig. 5-4

BAM	Plan of measurement points for fire test	Ref. 1.02

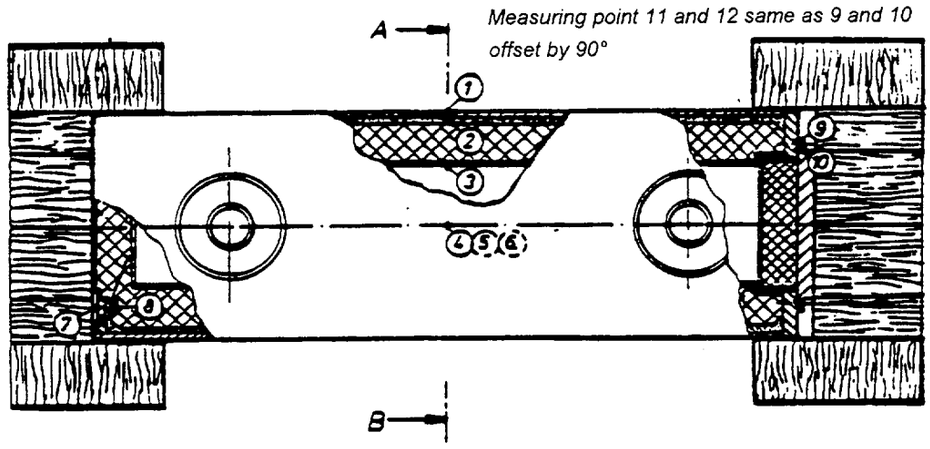

Section "A - B'

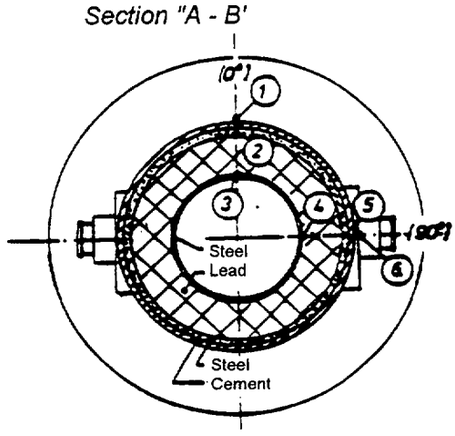

Meas. point	Situation or position of the measuring point	
1	Exterior mantle, centre of cask	[0°]
2	Lead shielding (exterio) centre of cask	[0°]
3	Lead shielding (interior) centre of cask	[0°]
4	Exterior mantle, centre of cask	[90°]
5	Lead shielding (exterior) centre of cask	[90°]
6	Lead shielding (interior) centre of cask	[90°]
7	Bottom valve (upper area)	
8	Bottom valve (lower area)	
9	Lid gasket -1a-	[0°]
10	Lid gasket -1b-	[0°]
11	Lid gasket -1a-	[90°]
12	Lid gasket -1b-	[90°]

Fig. 5-5

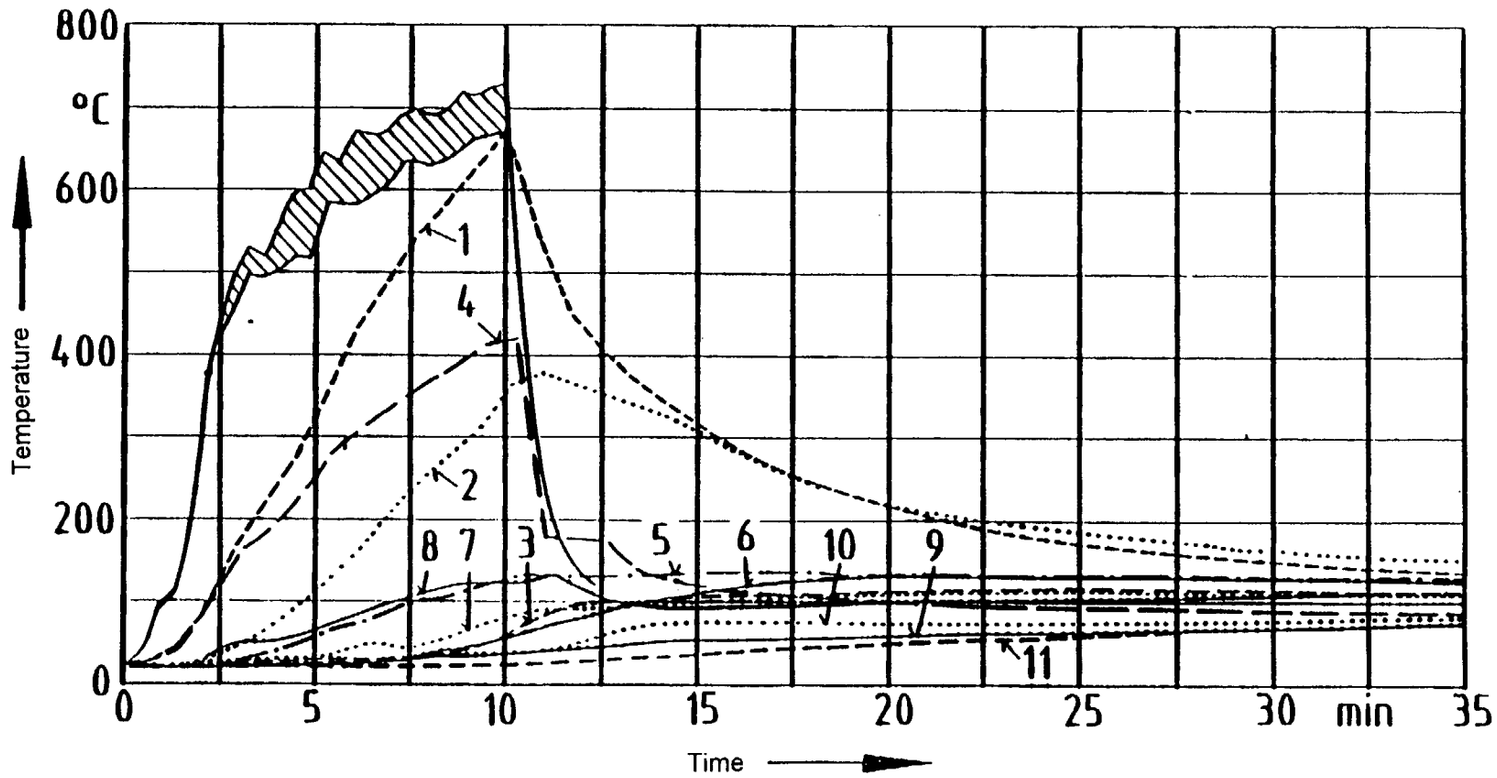

BAM Ref. 1.02

Time dependence of temperature for a TN 7-2 1/3 scale model during fire test

Fig. 5-6

6. Tightness of cask

It is verified that the activity leak rate L of the cask remains below the limit values valid according to traffic regulations for a type B(U) cask, both under normal operating conditions and under accidental conditions.

According to /6-1/, the admissible limits are:

Normal conditions:

$$L \cong 10^{-6} \cdot A_2/h$$

Accidental conditions:

$$L \cong 10^{-3} \cdot A_2/week$$

6.1 Initial data for verification

- The tightness system of the cask, which consists of three tightening points, has a leak rate of:

  $$L_0 \cong 1.33 \cdot 10^{-4} \text{ bar} \cdot \text{cm}^3 \text{ s}^{-1} \ (\cong 10^{-4} \text{ Torr} \cdot \text{l} \cdot \text{s}^{-1})$$

  $$(L_0 \cong 3 \cdot 10^{-5} \text{ Torr} \cdot \text{l} \cdot \text{s}^{-1} \text{ per gasket})$$

- Leak rates remain below this value, even under accidental conditions, as shown in drop tests.

- When preparing the cask for transport, an underpressure of 0.6 bar (related to temperature equilibrium) is established in the cask cavity, so as to create an inwards flowing gas stream.

- Fission gas inventory releases in MTR fuel assemblies (U-Al alloys) are negligible according to /6-2/ and /6-3/, as long as temperature remains below melting temperature.

  Measurements carried out on the TN 7 cask loaded with 15 MERLIN and 45 DIDO fuel assemblies, of which some merely had the shortest cooling time permissible for transport, revealed no fission gases under operating conditions.

  Although the melting temperature of the fuel assemblies is not reached, even in a fire, according to /6-4/, a release of 5 % of fission gases contained in the fuel assemblies is assumed under accidental conditions.

6.2 Verification methods

It is certified that under normal conditions underpressure inside the cask is maintained, so that no release of activity from the inside to the environment can occur.

Under accidental conditions, a release of 5 % of fission gases is assumed, based on /6-4/. It can however be verified that underpressure is maintained inside the cask even under accidental conditions.

6.3 Composition of fission gas

Only those nuclides are considered which are volatile at temperatures below the maximum fuel pin temperatures.

A. Loading with DIDO and MERLIN fuel assemblies

Calculation of the radioactive inventory was carried out in /6-5/. It will be presented briefly here.

The most unfavourable case of load is that of 60 DIDO fuel assemblies. The number of fissile U atoms in the cask then is:

$$No_{25} = \frac{60 \cdot 185 \cdot 6.02 \cdot 10^{23}}{235} = 2.84 \cdot 10^{25}$$

For a neutron flux of $\varnothing = 10^{14}$ n/sec · cm^2 (average flux) and a

period of irradiation $\tau = 6 \cdot 10^6$ sec,

one obtains according to /6-6/ the following fission gas inventory (stable and long lived radioactive isotopes):

Isotope	N_τ/No_{25}
Br 81	$7 \cdot 10^{-5}$
Kr 82	$5 \cdot 10^{-7}$
Kr 83	$1.5 \cdot 10^{-3}$
Kr 84	$4 \cdot 10^{-3}$
Kr 85	$1.1 \cdot 10^{-3}$
Kr 86	$7 \cdot 10^{-3}$
J 127	$6.5 \cdot 10^{-4}$
J 129	$3 \cdot 10^{-3}$
Xe 131	$8 \cdot 10^{-3}$
Xe 132	$1.5 \cdot 10^{-2}$
Xe 134	$2.5 \cdot 10^{-2}$
Xe 136	$4 \cdot 10^{-2}$
Sum	0.105

$\Sigma N_\tau = 0.105 \cdot 2.84 \cdot 10^{25} = 3.0 \cdot 10^{24}$ gas atoms in the fuel assemblies

B. RHF fuel assemblies

The fission gas inventory is determined as above according to /6-5/ and /6-6/.

$$No_{25} = \frac{2 \cdot 8556 \cdot 6.02 \cdot 10^{23}}{235} = 4.38 \cdot 10^{25} \text{ U-235 atoms}$$

For a neutron flux of $\varnothing = 1.5 \cdot 10^{14}$ n/sec · cm^2 (average flux) and a

period of irradiation $\tau = 44$ d $= 3.8 \cdot 10^6$ sec,

one obtains the following fission gas inventory (stable and long lived radioactive isotopes):

Isotope	N_τ/No_{25}
Br 81	$7 \cdot 10^{-5}$
Kr 82	$5 \cdot 10^{-7}$
Kr 83	$1.6 \cdot 10^{-3}$
Kr 84	$4 \cdot 10^{-3}$
Kr 85	$1.0 \cdot 10^{-3}$
Kr 86	$7.5 \cdot 10^{-3}$
J 127	$5.5 \cdot 10^{-4}$
J 129	$2.8 \cdot 10^{-3}$
Xe 131	$7 \cdot 10^{-3}$
Xe 132	$1.5 \cdot 10^{-2}$
Xe 134	$2.7 \cdot 10^{-2}$
Xe 136	$4.3 \cdot 10^{-2}$
Sum	0.109

$\Sigma N_\tau = 0.109 \cdot 4.38 \cdot 10^{25} = 4.77 \cdot 10^{24}$ gas atoms in the fuel assemblies

6.4 Tightness under normal conditions

With an assumed transport duration of t = 100 d (this is very conservative as in general transports last 20 days at the utmost), the pressure increase Δp is conservatively calculated in a simplified manner as follows:

$$\Delta p = \frac{L \cdot t}{V} = \frac{1.33 \cdot 10^{-4} \cdot 8.64 \cdot 10^{6}}{4.38 \cdot 10^{5}} = 2.6 \cdot 10^{-3} \text{ bar}$$

$V = 438 \text{ l} = 4.38 \cdot 10^{-5} \text{ cm}^3$ (minimum free cask volume)

$p_1 = p_0 + \Delta p = 0.6 \text{ bar} + 2.6 \cdot 10^{-3} \text{ bar}$

$p1 \approx = 0.6027$ bar = interior pressure in the cask after 100 d.

Pressure increases due to the leak rate of the tightening system during the considered 100 d is negligible.

According to conservative calculations, time required until pressure equilibrium is established is:

$$t = \frac{\Delta p \cdot V}{L} = -\frac{0.4 \cdot 4.38 \cdot 10^{5}}{1.33 \cdot 10^{-4}}$$

$t = 1.3 \cdot 10^{9} \text{ sec} \cong 41.8 \text{ years}$

The gas flow is directed inward during a practically unlimited period of time, which means that no activity release occurs.

Before every transport, a leak rate of

$L \cong 1 \cdot 10^{-2} \text{ bar cm}^3 \cdot \text{s}^{-1}$

is verified for the cask, so that maintenance of underpressure is assured within a transport period of 100 days.

$$\Delta p = \frac{1.10 \cdot 10^{-2} \cdot 8.64 \cdot 10^{6}}{4.38 \cdot 10^{5}} = 0.20 \text{ bar}$$

$$p_1 = p_0 + \Delta p = 0.6 + 0.2 = 0.8 \text{ bar}$$

6.5 Tightness under accidental conditions

It is assumed that 5 % of the fission gas inventory is released (according to /6-4).

In case of fire, the average air temperature inside the cask increases by 150 K according to conservative estimates.

A. DIDO and MERLIN fuel assemblies

- Pressure increase due to fission gases

For a release of 5 %, the amount of gas atoms released into the cask is:

$$Z = 0.05 \cdot 3.0 \cdot 10^{24} = 1.5 \cdot 10^{23}$$

The resulting pressure increase Δp is:

$$\Delta p = \frac{Z \cdot R \cdot T_0}{V \cdot L}$$

with: $R = 8.315 \ \frac{J}{mole\,K}$ = general gas constant

$L = 6.02 \quad 10^{23}$ 1/mole

$V = 0.438 \ m^3$

$T_0 = 573$ K (average air temperature in the cask, conservative assumption)

$\Delta p = 2.71 \cdot 10^3 \ N/m^2 = 0.027$ bar ($\cong$ 20.3 Torr)

Pressure inside the cask after release of fission gases:

$$p_2 = p_1 + \Delta p = 0.6027 + 0.027 = 0.63 \text{ bar}$$

- Maximum pressure in the cask due to an accidental fire:

$$p_3 = \frac{T_1}{T_0} \cdot p_2$$

$$p_3 = \frac{723}{573} \cdot 0.63 = 0.80 \text{ bar}$$

The maximum expected interior pressure remains below ambient atmospheric pressure, so that no leak occurs.

B. RHF fuel assemblies

- Pressure increase due to fission gases

For a release of 5 %, the amount of gas atoms released into the cask is:

$$Z = 0.05 \cdot 4.77 \cdot 10^{24} = 2.385 \cdot 10^{23}$$

$$\Delta p = \frac{Z \cdot R \cdot T_0}{V \cdot L} = \frac{2.385 \cdot 10^{23} \cdot 8.135 \cdot 537}{0.509 \cdot 6.02 \cdot 10^{23}}$$

$$p = 3.63 \cdot 10^3 \text{ N/m}^2 = 0.0363 \text{ bar}$$

with: $T_0 = 573$ K = average air temperature in the cask according to conservative estimates

$$p_2 = p_1 + \Delta p = 0.6027 \cdot 0.0363$$

$$p_2 = 0.64 \text{ bar}$$

- Maximum pressure in the cask due to an accidental fire

$$p_3 = \frac{T_1}{T_0} \cdot p_2$$

$$= \frac{723}{573} \cdot 0.64 = 0.81 \text{ bar}$$

The maximum expected interior pressure remains below ambient atmospheric pressure, so that no leak occurs.

6.6 Literature

/6-1/ IAEA-Regulations for the Safe Transport of Radioactive Materials, 1973

/6-2/ M. B. Reynolds,
Fission Gas Behaviour in the U-Al System,
Nucl. Sc. and Eng., 3, 1958

/6-3/ H. W. Castleman et al.
"Diffusion of Xe through Al and stainless steel",
BNL 624, 1960

/6-4/ P. Rocco, IAEA-SR-10/43

/6-5/ TN 7/MTR Package Design, Safety Report,
TN Report No. 7701

/6-6/ I. O. Blomeke/M. F. Todd
U-235 Fission Product Production as a Function of Thermal Neutron Flux, Irradiation Time and Decay Time,
ORNL 2127, Oak Ridge

7. Dose rate at cask surface

It is demonstrated that under normal transport conditions and accidental conditions, the dose rate (DR) at the surface of the cask remains below the admissible limits according to traffic regulations based on IAEA Rules /7-7/:

Normal conditions:	surface	DR ≅ 200 mrem/h
	2 m distance	DR ≅ 10 mrem/h
Accidental conditions:	1 m distance	DR ≅ 1000 mrem/h

7.1 Structure of shielding

Shielding thicknesses indicated below are maintained also after the testing conditions for type B casks, as already verified in chapter 4.5. The cement layer in the mantle dehydrates. Conservatively, the shielding effect of this layer under accidental conditions is negligible.

- Cask mantle
  (cf. Fig. 7-1)

Table 7-1: shielding thicknesses in the cask mantle

Material	Shielding thickness t (cm)	Density (g/cm^3)
Steel	1.0	7.90
Lead	18.5	11.2
Cement	2.0 [1)]	1.89
Steel	2.5	7.90

[1)] Minimum thickness of the cement layer

- Shielding of the end surfaces
  (cf. Fig. 7-1)

Table 7-2: Shielding thicknesses on the lid end

Material	Shielding thickness t (cm)
Steel	1.0
Lead	16.5
Steel	7.0

Table 7-3: Shielding thicknesses on the bottom end

Material	Shielding thickness t (cm)
Steel	1.75 [1)]
Lead	17.0
Steel	2.5

[1)] Average thickness of the bottom

The shock absorbers are not included in the calculation of the shielding of the front end. These results are thus conservative.

7.2 Source intensities

The MTR fuel assemblies which are to be transported only have negligible neutron source intensities. Only gamma sources must be taken into account for shielding calculations.

A. DIDO and MERLIN fuel assemblies

According to /7-1/, the source intensity with a load of 4 DIDO insert baskets is identical to that with 3 DIDO and 1 MERLIN insert baskets, which means that in this case the same values may be expected. Gamma source intensities according to /7-1/ are taken, as the same conditions apply (cf. also chapter 2.5):

Power per fuel assembly: 1.0 $_{MWth}$/assembly
Irradiation period: t_B = 70 d = $6 \cdot 10^6$ sec
Cooling time: t_A = 231 d = $2 \cdot 10^7$ sec

The cooling time is averaged in such a way that thermal power per insert basket remains below 1125 W.

Source intensities were obtained from /7-2/.

Following source intensities are found:

Table 7-4a: Gamma source intensities of DIDO and MERLIN fuel assemblies

Energy group	Source intensity S/cask (1/sec)	Volume source intensity S_V (1/s · cm^3)
1 - 1.7 MeV (reference energy 1.5 MeV)	$1.32 \cdot 10^{14}$	$2.34 \cdot 10^8$
> 1.7 MeV (reference energy 2.0 MeV)	$5.28 \cdot 10^{13}$	$9.35 \cdot 10^7$

The volume source intensity of the fuel assemblies homogenised in the interior cask cavity is calculated according to:

$$S_V = \frac{S}{R_0^2 \cdot \pi \cdot h}$$

with: R_0 = 26 cm = radius of insert baskets
H = 266 cm = height of the four insert baskets

B. RHF fuel assemblies

The source intensities are taken from /7-3/, as the initial conditions for the fuel assemblies are the same.
Total source intensities were assessed according to /7-2/.

Power per fuel assembly:	P	=	0.25 MW_{th}/assembly
Irradiation time:	t_B	=	44 d = $3.8 \cdot 10^6$ sec
Cooling time:	t_A	=	310 d = $2.68 \cdot 10^7$ sec

The following source intensities result:

Table 7-4b: Gamma source intensities of RHF fuel assemblies

Energy group	Source intensity S/cask (1/sec)	Source intensity S of the linear source (1/sec)	Source intensity S_L per unit length (1/sec)
1 - 1.7 MeV (ref. energy 1.5 MeV)	$1.28 \cdot 10^{14}$	$8 \cdot 10^{12}$	$3.96 \cdot 10^{10}$
> 1.7 MeV (ref. energy 2.0 MeV)	$1.90 \cdot 10^{13}$	$1.19 \cdot 10^{13}$	$5.89 \cdot 10^{9}$

Homogeneous fuel distribution is assumed within the fuel assembly annulus. This annulus is subdivided into 16 linear sources (Fig. 7-2). The source intensity of the linear source is calculated according to:

$$S_L = \frac{S}{16 \cdot H}$$

with: H = 202 cm (height of the 2 fuel assemblies including the distance between them)

7.3 Calculation methodology

A. DIDO and MERLIN fuel assemblies

Calculation of dose rates at the mantle and the front ends is carried out applying Rockwell's volume source model /7-4/. Fuel assemblies and insert basket parts in the volume of cylinder sources are homogenised.

Calculation is carried out according to the following equations:

- Maximum dose rates at the mantle (central plane)

$$D = U \cdot \frac{B \cdot S_V}{4 \cdot (a+z)} \cdot F(\theta, b_2)$$

- Maximum dose rate at the front ends ("upper limit": $h \cong \frac{3}{\mu_s}$)

$$D = U \cdot \frac{B \cdot S_V}{2 \cdot \mu_s} \cdot \left[E_2(b) - \frac{E_2(b \cdot \sec\theta)}{\sec\theta} \right]$$

with:

U	=	conversion factor for the assessment of the dose rate from the flux of gamma quanta (mrem · h-1 · cm2 · sec)
B	=	build-up factor
S_V	=	volume source intensity /1/s · cm^3)
$F(\theta, b_2)$	=	attenuation factor according to table in /7-4/
$\tan\theta$	=	$\frac{H}{a+z}$ (mantle), $\tan\theta = \frac{R_0}{a}$ (front ends)
H	=	source height
a	=	distance between source and point of calculation
b	=	length of relaxation = $\Sigma\mu_i \cdot t_i$
b_2	=	$b + \mu_s \cdot z$

μ_i = macroscopic cross-section of shielding element i (according to /7-5/)

t_i = thickness of shielding element i

z = thickness of source self-shielding according to /7-4/

μ_s = macroscopic cross-section of the source. The latter consists of the fuel assemblies and the corresponding parts of the insert baskets.

$\mu_s = \left(\sum \frac{\mu_i}{d_i} \cdot \frac{A_i}{100}\right) \cdot d_s$

A_i = % weight participation of fuel assembly i in the source

d_s = density of the homogenised source

$E_2(b) - \frac{E_2(b \cdot \sec\theta)}{\sec\theta}$ This expression is determined from graphs in /7-4/.

Values μ_s and μ_i/d_i are represented in tables further on.

B. RHF fuel assemblies

Calculation of dose rates at the mantle and the front ends is carried out similarly to /7-3/ according to Rockwell's linear source model, with source intensities determined in 7.2. Self-shielding in the linear sources is taken into account.

The calculation model permits:

- taking into account of the different distances between the single sources and the receiving point;

- taking into account of shielding thickness increase due to radiation traversing the cask walls askew.

Geometric conditions are described in fig. 7-3. The following equation applies:

- Maximum dose rate at the mantle (central plane)

$$D = U \cdot \frac{B \cdot S_{LS}}{2 \cdot \pi \cdot a} \cdot F(\theta_1, b_1) \text{ with } a = 1_3$$

- Maximum dose rate at the front ends ($h \cong \frac{3}{\mu_s}$)

$$D = U \cdot \frac{B \cdot S_{LS}}{4 \cdot \pi \cdot a} \cdot [F(\theta_1, b_1) - (F(\theta_2, b_2)]$$

$$S_{LS} = \frac{S_L}{\alpha} \cdot (1 - \frac{1}{e^{\alpha}})$$

with S_L according to chapter 7.2.

$\alpha = \mu_S \cdot a$ (μ_S according to table 7-5, a = 6.8 cm, cf. fig. 7-2),

the signification of every factor being the same as described under 7.3A. The effective b-value for the single linear sources at the mantle is determined according to the following method:

$$b_{eff} = b' \cdot \frac{1_2 - 1_1}{r_a - r_i}$$

with b' = b for sources 1 - 8
b' = b + t · μ_S for sources 9 - 16
(b according to tables 7-6 till 7-8; μ_S according to table 7-5)

t = 6.8 cm (cf. fig. 7-2)

The b_{eff} values, build-up factors and $F(\theta, b)$ values are listed in tables 7-10 and 7-11 for the single linear sources.

Only one side of the annulus is considered, for reasons of symmetry, that is linear sources 1 - 4 and 9 - 12. Total dose rate is then calculated from the sum of the single dose rates of the considered linear sources, multiplied by 2.

7.4 Initial data

7.4.1 Cross sections for gamma radiation

The values for macroscopic cross-sections μ (cm^{-1}) of shielding materials are determined based on the mass attenuating coefficients μ/ρ (cm^2/g) according to /7-5/.

The values μ/ρ, μ and b are represented in tables 7-6, 7-7 and 7-8.

7.4.2 Build-up factor

The values for build-up B are determined according to Broder's method /7-6/, p. 231.

7.4.3 Conversion factor

The conversion factor U to determine dose rates based on the flux is found in /7-6/ (cf. table 7-9).

Table 7-5: Macroscopic cross-section μ_S of the source

A. DIDO and MERLIN fuel assemblies

Energy group (MeV)	1,5	2,0
μ_{Fe}/ρ_{Fe}	0,0485	0,0424
μ_U/ρ_U	0,0548	0,0484
μ_{Al}/ρ_{Al}	0,0500	0,0432
μ_S	0,0596	0,0520

ρ_S = 1,22 g/cm³

The bottom plates of the insert baskets were neglected because they are not oriented in the direction of radiation.

The weight of the source is composed of:

- 60 fuel assemblies:
  12 kg uranium
  + 150 kg aluminum
  162 kg
- 4 insert baskets:
  + 580 kg steel
  - 54 kg steel (bottom plates)
  688 kg

B. RHF fuel assemblies

Energy group (MeV)	1,5	2,0
μ_U/ρ_U	0,0548	0,0484
μ_{Al}/ρ_{Al}	0,0500	0,0432
μ_S/ρ_S	0,0504	0,0436
μ_S	0,0806	0,0698

ρ_S = 1.6 g/cm³
density of the homogenised annulus

Table 7-6: Cross sections, relaxation lengths and build-up factors for dose rate calculation at the mantle

E-group	Material	Steel	Lead	Cement	b	B
	t (cm)	3,5	18,5	2,0		
	μ/ϱ (cm^2/g)	0,0485	0,0512	0,0517		
1,5 MeV	μ (cm^{-1})	0,3832	0,5734	0,0982	12,15	6,72
	$\mu \cdot t$ (-)	1,3410	10,6086	0,1965		
	μ/ϱ (cm^2/g)	0,0424	0,0457	0,0445		
2,0 MeV	μ (cm^{-1})	0,3350	0,5118	0,0846	10,81	5,73
	$\mu \cdot t$ (-)	1,1724	9,4690	0,1691		

Table 7-6: Cross sections, relaxation lengths and build-up factors for dose rate calculation at the lid

E-group	Material	Steel	Lead	b	B
	t (cm)	8,0	16,5		
	μ/ϱ (cm^2/g)	0,0485	0,0512		
1,5 MeV	μ (cm^{-1})	0,3832	0,5734	12,53	7,36
	$\mu \cdot t$ (-)	3,0652	9,4618		
	μ/ϱ (cm^2/g)	0,0424	0,0457		
2,0 MeV	μ (cm^{-1}	0,3350	0,5118	11,13	6,34
	$\mu \cdot t$ (-)	2,6797	8,4454		

Table 7-8: Cross sections, relaxation lengths and build-up factors for dose rate calculation at the bottom

E-group	Material	Steel	Lead	b	B
	t (cm)	4,25	17,0		
	μ/ϱ (cm^2/g)	0,0485	0,0512		
1,5 MeV	μ (cm^{-1})	0,3832	0,5734	11;38	6,25
	$\mu \cdot t$ (-)	1,6284	9,7485		
	μ/ϱ (cm^2/g)	0,0424	0,0457		
2,0 MeV	μ (cm^{-1})	0,3350	0,5118	10,12	5,41
	$\mu \cdot t$ (-)	1,4236	8,7013		

Table 7-9: Conversion factor U for gamma radiation

E-group (MeV)	Reference energy (MeV)	Conversion factor ($mR \cdot h^{-1} \cdot s \cdot cm^2$)
1,5	1,5	$2,65 \cdot 10^{-3}$
2,0	2,0	$3,2 \cdot 10^{-3}$

Table 7-10: Initial data for dose rate calculations at the mantle surface (cask loaded with 2 RHF fuel assemblies)

Source Nr.	l_2-l_1 (cm)	l_3 (cm)	θ	E-group (MeV)	b'	b_{eff}	B	$\Delta F(\theta,b)$
1	27,5	51,0	63,2	1,5	12,15	13,64	7,5	$3,88 \cdot 10^{-7}$
				2,0	10,81	12,13	6,4	$1,85 \cdot 10^{-6}$
2	27,3	44,4	66,3	1,5	12,15	13,54	7,5	$4,30 \cdot 10^{-7}$
				2,0	10,81	12,05	6,4	$2,01 \cdot 10^{-6}$
3	26,0	38,7	69,0	1,5	12,15	12,89	7,1	$8,42 \cdot 10^{-7}$
				2,0	10,81	11,47	6,1	$3,67 \cdot 10^{-6}$
4	24,7	35,2	70,8	1,5	12,15	12,25	6,8	$1,63 \cdot 10^{-6}$
				2,0	10,81	10,90	5,8	$6,65 \cdot 10^{-6}$
9	26,8	57,2	60,5	1,5	12,70	13,89	7,7	$2,99 \cdot 10^{-7}$
				2,0	11,28	12,34	6,5	$1,49 \cdot 10^{-6}$
10	25,8	62,4	58,3	1,5	12,70	13,37	7,4	$5,13 \cdot 10^{-7}$
				2,0	11,28	11,88	6,3	$2,40 \cdot 10^{-6}$
11	25,0	66,1	56,8	1,5	12,70	12,96	7,2	$7,83 \cdot 10^{-7}$
				2,0	11,28	11,51	6,1	$3,53 \cdot 10^{-6}$
12	24,6	68,0	56,0	1,5	12,70	12,75	7,0	$9,74 \cdot 10^{-7}$
				2,0	11,28	11,33	6,0	$4,25 \cdot 10^{-6}$

Table 7-11: Initial data for dose rate calculations at the mantle, at 2 m distance (cask loaded with 2 RHF fuel assemblies)

Source Nr.	l_2-l_1 (cm)	l_3 (cm)	θ	E-group (MeV)	b'	b_{eff}	B	$\Delta F(\theta,b)$
1	27,5	248,8	22,1	1,5	12,15	13,64	7,5	$3,39 \cdot 10^{-7}$
				2,0	10,81	12,13	6,4	$1,58 \cdot 10^{-6}$
2	26,6	242,6	22,6	1,5	12,15	13,19	7,3	$5,42 \cdot 10^{-7}$
				2,0	10,81	11,74	6,2	$2,38 \cdot 10^{-6}$
3	25,4	237,7	23,0	1,5	12,15	12,60	7,0	$9,97 \cdot 10^{-7}$
				2,0	10,81	11,21	5,9	$4,12 \cdot 10^{-6}$
4	24,6	235,1	23,2	1,5	12,15	12,20	6,7	$1,50 \cdot 10^{-6}$
				2,0	10,81	10,85	5,7	$5,98 \cdot 10^{-6}$
9	27,3	255,3	21,6	1,5	12,70	14,15	7,8	$2,0 \cdot 10^{-7}$
				2,0	11,28	12,57	6,7	$9,98 \cdot 10^{-7}$
10	26,3	261,2	21,1	1,5	12,70	13,63	7,5	$3,35 \cdot 10^{-7}$
				2,0	11,28	12,12	6,4	$1,56 \cdot 10^{-6}$
11	25,2	265,6	20,8	1,5	12,70	13,06	7,2	$5,94 \cdot 10^{-7}$
				2,0	11,28	11,60	6,1	$2,62 \cdot 10^{-6}$
12	24,6	268,0	20,6	1,5	12,70	12,75	7,0	$8,10 \cdot 10^{-7}$
				2,0	11,28	11,33	6,0	$3,44 \cdot 10^{-6}$

7.5 Calculation and results

7.5.1 Dose rates under normal transport conditions

7.5.1.1 Mantle dose rate

The maximum mantle dose rate is calculated for a point situated at the centre of the active zone. The active length was not subdivided into zones.

A. DIDO and MERLIN fuel assemblies

- Geometry for the calculation of the surface dose rate

H = 266 cm = height of source

a = 25 cm = distance between source and point of calculation

R_0 = 26 cm = radius of source

$$\tan\theta = \frac{H/2}{a+z} = \frac{266/2}{25/z}$$

- Geometry for the calculation of the dose rate at a distance of 2 m

H = 266 cm = height of source

a = 225 cm = distance between source and point of calculation

R_0 = 26 cm = radius of source

$$\tan\theta = \frac{H/2}{a+z} = \frac{266/2}{225/z}$$

The results of calculations are given below.

Table 7-12a: Mantle dose rate calculation for DIDO and MERLIN fuel assemblies

Point of calculation at the cask	Surface		2 m distance	
E-group (MeV)	1,5	2,0	1,5	2,0
U ($mrem \cdot h^{-1} \cdot sec \cdot cm^2$)	$2,65 \cdot 10^{-3}$	$3,2 \cdot 10^{-3}$	$2,65 \cdot 10^{-3}$	$3,2 \cdot 10^{-3}$
B	6,72	5,73	6,72	5,73
S_v ($1/s \cdot cm^3$)	$2,34 \cdot 10^{8}$	$9,35 \cdot 10^{7}$	$2,34 \cdot 10^{8}$	$9,35 \cdot 10^{7}$
μ_S (cm^{-1})	0,0596	0,0520	0,0596	0,0520
b	12,15	10,81	12,15	10,81
Z (cm)	22,59	22,73	18,60	19,92
θ (°C)	70,31	70,26	28,66	28,53
b_2	13,49	11,99	13,17	11,78
$\Delta F(\theta, b_2)$	$4,35 \cdot 10^{-7}$	$2,14 \cdot 10^{-6}$	$6,02 \cdot 10^{-7}$	$2,51 \cdot 10^{-6}$
D (mrem/h)	13,1	25,5	3,5	5,9
D_{Ges} (mrem/h)	38,6		9,4	

B. RHF fuel assemblies

- Geometry for the calculation of the surface dose

H = 202 cm = height of source

a = l_3: cf. table 7-10 = distance between source and point of calculation

U : cf. table 7-9

B : cf. table 7-10

F(θ, b) : cf. table 7-10

S_{LS} = $S_L \cdot 0.77$ (1.5 MeV)
= $S_L \cdot 0.796$ (2.0 MeV)

Table 7-12b: Dose rate at the mantle surface for 2 RHF fuel assemblies (mrem/h)

Source no.		1	2	3	4	9	10	11	12
D	1,5(MeV)	0,73	0,93	1,99	4,05	0,52	0,79	1,09	1,29
	2,0(MeV)	0,58	0,72	1,45	2,74	0,42	0,61	0,81	0,94
$D_1=\sum D$		1,31	1,65	3,44	6,79	0,94	1,40	1,90	2,23

$D_{Ges} = 2 \cdot D_1 = 2 \cdot 19,66$

$D_{Ges} = 39,3$ mrem/h

- Geometry for the calculation of the dose rate at a distance of 2 m

a = l_3: cf. table 7-11 = distance between source and point of calculation

U : cf. table 7-9

B : cf. table 7-11

F(θ, b) : cf. table 7-11

S_{LS} = cf. above

Table 7-12c: Mantle dose rate at 2 m distance for 2 RHF fuel assemblies (mrem/h)

Source no.		1	2	3	4	9	10	11	12
D	1,5(MeV)	0,13	0,21	0,38	0,55	0,08	0,12	0,21	0,27
	2,0(MeV)	0,10	0,15	0,25	0,37	0,06	0,10	0,15	0,19
D_1		0,23	0,36	0,63	0,92	0,14	0,22	0,36	0,46

$D_{Ges} = 2 \cdot D_1 = 2 \cdot 3,32$

$D_{Ges} = 6,6$ mrem/h

7.5.1.2 Dose rate at the lid

Dose rates are determined at the surface of the lid and at a distance of 2 m according to the equations in chapter 7.3. The active zone is considered as a total zone for calculations.

A. DIDO and MERLIN fuel assemblies

- Geometry for the calculation of dose rate at the surface

H = 266 cm = height of source

a = 24.5 cm = distance between source and point of calculation

R_0 = 26 cm = radius of source

$$\tan\theta = \frac{R_0}{a}$$

- Geometry for the calculation of dose rate at 2 m distance

H = 266 cm = height of source

a = 224.5 cm = distance between source and point of calculation

R_0 = 26 cm = radius of source

$$\tan\theta = \frac{R_0}{a}$$

Calculation results are given in the following table.

Table 7-13a: Dose rate calculation at the lid for DIDO and MERLIN fuel assemblies

Point of calculation at the cask	Surface		2 m distance	
E-group (MeV)	1,5	2,0	1,5	2,0
S_V (1/s·cm³)	$2,34 \cdot 10^{8}$	$9,35 \cdot 10^{7}$	$2,34 \cdot 10^{8}$	$9,35 \cdot 10^{7}$
U (mrem·h^{-1}·sec·cm²)	$2,65 \cdot 10^{-3}$	$3,2 \cdot 10^{-3}$	$2,65 \cdot 10^{-3}$	$3,2 \cdot 10^{-3}$
B (-)	7,36	6,34	7,36	6,34
θ (°C)	46,70	46,70	6,61	6,61
μ_S (cm^{-1})	0,0596	0,0520	0,0596	0,0520
b (-)	12,53	11,13	12,53	11,13
ΔE (θ,b)	$2,51 \cdot 10^{-7}$	$1,09 \cdot 10^{-6}$	$2,27 \cdot 10^{-8}$	$8,89 \cdot 10^{-8}$
D (mrem/h)	9,6	19,9	0,9	1,6
D_{Ges} (mrem/h)	29,5		2,5	

B. RHF fuel assemblies

Calculations must only be carried out for a linear source. Total result D_{GES} is obtained by multiplying by 16. Self shielding is taken into account at the mantle. The calculation model is represented in Fig. 7-4.

$$\tan\theta_1 = \frac{a}{x}; \quad \tan\theta_2 = \frac{a}{x+1}$$

$b_1 = b + \mu_{Fe} \cdot S$

b : according to table 7-7

S = thickness of spacer plate = 1.5 cm

- Geometry for dose rate calculation at the surface

l = H = 202 cm = height of source

a = 16,785 cm = distance between source and cask central axis

x = 59 cm = distance between source and point of calculation

- Geometry for dose rate calculation at 2 m distance

l = H = 202 cm = height of source

a = 16,785 cm = distance between source and cask central axis

x = 59 + 200 = 259 cm = distance between source and point of calculation

The results are displayed below.

Table 7-13b: Dose rate calculation at the lid for 2 RHF fuel assemblies

Calculating point at cask	Surface		2 m distance	
E-group (MeV)	1,5	2,0	1,5	2,0
S_{LS} (1/s·cm)	$3{,}05 \cdot 10^{10}$	$4{,}69 \cdot 10^{9}$	$3{,}05 \cdot 10^{10}$	$4{,}69 \cdot 10^{9}$
U (mrem·h^{-1}·sec·cm^2)	$2{,}65 \cdot 10^{-3}$	$3{,}2 \cdot 10^{-3}$	$2{,}65 \cdot 10^{-3}$	$3{,}2 \cdot 10^{-3}$
B (-)	7,36	6,34	7,36	6,34
b	12,53	11,13	12,53	11,13
b_1 (-)	13,10	11,63	13,10	11,63
$\triangle F(\theta, b_1)$	$3{,}53 \cdot 10^{-7}$	$1{,}57 \cdot 10^{-6}$	$5{,}68 \cdot 10^{-8}$	$2{,}48 \cdot 10^{-7}$
D (mrem/h)	0,996	0,708	0,160	0,112
D_{Ges} (mrem/h)	27,3		4,4	

7.5.1.3 Dose rate at the bottom

Calculation is carried out similarly to the way described in chapter 7.3. Dose rate is determined for the central cask axis at the bottom and at a distance of 2 m. The active length is considered as total zone.

A. DIDO and MERLIN fuel assemblies

- Geometry for the calculation of the surface dose rate

H = 266 cm = height of source

a = 21.25 cm = distance between source and point of calculation

R_0 = 26 cm = radius of source

$$\tan\theta = \frac{R_0}{a}$$

- Geometry for the calculation of the dose rate at a distance of 2 m

H = 266 cm = height of source

a = 221.25 cm = distance between source and point of calculation

R_0 = 26 cm = radius of source

$$\tan\theta = \frac{R_0}{a}$$

The results of calculations are given in the following table.

Table 7-14a: Dose rate calculation at the bottom for DIDO and MERLIN fuel assemblies

Calculating point at cask	Surface		2 m distance	
E-group (MeV)	1,5	2,0	1,5	2,0
S_V (1/s·cm³)	$2{,}34 \cdot 10^{8}$	$9{,}35 \cdot 10^{7}$	$2{,}34 \cdot 10^{8}$	$9{,}35 \cdot 10^{7}$
U (mrem·h^{-1}·sec·cm²)	$2{,}65 \cdot 10^{-3}$	$3{,}2 \cdot 10^{-3}$	$2{,}65 \cdot 10^{-3}$	$3{,}2 \cdot 10^{-3}$
B (-)	6,25	5,41	6,25	5,41
μ_S (cm^{-1})	0,0596	0,0520	0,0596	0,0520
b (-)	11,38	10,12	11,38	10,12
ΔE (θ,b)	$8{,}40 \cdot 10^{-7}$	$3{,}15 \cdot 10^{-6}$	$7{,}16 \cdot 10^{-8}$	$2{,}42 \cdot 10^{-7}$
D (mrem/h)	27,3	49,0	2,3	3,8
D_{Ges} (mrem/h)	76,3		6,1	

B. RHF fuel assemblies

Calculation as for the lid.

$b_1 = b + \mu_{Fe} \cdot S$

b = cf. table 7-8

S = 2.275 = equivalent shielding through insert basket bottoms

- Surface

l = H = 202 cm

a = 16.785 cm

- 2m distance

H = 202 cm

a = 16.785 cm

x = 251.75 cm

The results of calculations are shown below.

Table 7-14b: Dose rate calculation at the bottom for 2 RHF fuel assemblies

Calculating point at cask	Surface		2 m distance	
E-group (MeV)	1,5	2,0	1,5	2,0
S_{LS} (1/s·cm)	$3,05 \cdot 10^{10}$	$4,69 \cdot 10^{9}$	$3,05 \cdot 10^{10}$	$4,69 \cdot 10^{9}$
U (mrem·h^{-1}·sec·cm^2)	$2,65 \cdot 10^{-2}$	$3,2 \cdot 10^{-3}$	$2,65 \cdot 10^{-3}$	$3,2 \cdot 10^{-3}$
B (-)	6,25	5,41	6,25	5,41
b (-)	11,38	10,12	11,38	10,12
b_1 (-)	12,24	10,87	12,24	10,87
ΔE (θ,b)	$9,39 \cdot 10^{-7}$	$3,79 \cdot 10^{-6}$	$1,42 \cdot 10^{-7}$	$5,59 \cdot 10^{-7}$
D (mrem/h)	2,249	1,459	0,340	0,215
D_{Ges} (mrem/h)	59,3		8,9	

7.5.2 Dose rates under accidental conditions

The cement layer dehydrates under accidental conditions. It is conservatively assumed that the layer loses its shielding capacity due to this. The shock absorbers remain on the cask; however, they suffer deformations during an accident, so that they lose part of their shielding capacity. Dose rate calculations were, however, carried out without shock absorbers, so that this has no influence on the results. The usual shielding is remains unchanged. Calculations are carried out assuming a distance of 1 m from the cask.

7.5.2.1 Dose rate at the mantle surface

The maximum dose rate which occurs at the horizontal central plane is determined.

The new value of b is:

(1.5 MeV) b = 11.95 (as compared to 12.15 before)
(2.0 MeV) b = 10.64 (as compared to 10.81 before)

It is evident that the change of shielding capacity as compared to normal transport conditions is small.

All further values are considered to be constant (cf. chapter 7.5.1.1).

A. DIDO and MERLIN fuel assemblies

- Geometry for the calculation of the dose rate at a distance of 1 m of the mantle

  H = 266 cm = height of source

  a = 124.5 cm = distance between source and point of calculation

  R_0 = 26 cm = radius of source

  $$\tan\theta = \frac{H/2}{a+z}$$

  Except for the following values, all others coincide with the values used in 7.5.1.1:

  b_1 = 11.95 (1.5 MeV) b_2 = 13.31 (1.5 MeV)
  b_1 = 10.64 (2.0 MeV) b_2 = 11.71 (2.0 MeV)

  a = 124.5 cm
  Z = 22.82 (1.5 MeV) Z = 20.58 (2.0 MeV)

$\Delta F(\theta, b) = 5.45 \cdot 10^{-7}$ (1.5 MeV)

$\Delta F(\theta, b) = 2.86 \cdot 10^{-6}$ (2.0 MeV)

This yields a total dose rate at a distance of 1 m of the mantle of:

$D_{GES} = D_{1.5} + D_{2.0}$

$= 5.2 + 11.4 = 16.6$ mrem/h

B. RHF fuel assemblies

- 1m distance

The surface value is calculated by way of simplification.

The new dose rate value at the surface is calculated from:

$$\text{new } D_{GES} = D_{GES(1.5)} \cdot e^{\Delta b_{1.5}} + D_{GES(2.0)} \cdot e^{\Delta b_{2.0}}$$

$\Delta b_{1.5}$ = 0.2 (1.5 MeV)

$\Delta b_{2.0}$ = 0.17 (2.0 MeV)

$$D_{GES} = 22.78 \cdot e^{0.2} + 16.54 \cdot e^{0.17}$$

$$= 47.4 \text{ mrem/h}$$

The value for a distance of 1 m is lower than the calculated one.

7.5.2.2 Dose rate at the lid

Shielding is not changed under accidental conditions (if the shock absorbers are not taken into account). At the surface and at a distance of 2 m, the same values as in chapter 7.5.2.1 occur. Thus, values for a distance of 1 m are below the defined limit of 1000 mrem/h for all types of loads.

7.5.2.3 Dose rate at the bottom

The same applies for the bottom as for the lid.

7.6 Summary of results

The following tables summarise the calculated dose rates for the TN 7-2 cask, both under normal and accidental conditions.

It can be seen that the maximum dose rates which occur remain below the limits admitted by transport regulations.

Table 7-15a: Dose rates for the TN 7-2 loaded with DIDO and MERLIN fuel assemblies, under normal transport conditions (mrem/h)

Mantle		Lid		Bottom	
Surface	2 m	Surface	2 m	Surface	2 m
38.6	9.4	29.5	2.5	76.3	6.1

Table 7-15b: Dose rates for the TN 7-2 loaded with 2 RHF fuel assemblies, under normal transport conditions (mrem/h)

Mantle		Lid		Bottom	
Surface	2 m	Surface	2 m	Surface	2 m
39.3	6.6	27.3	4.4	59.3	8.9

Table 7-16a: Dose rates at a distance of 1 m of the TN 7-2 loaded with DIDO and MERLIN fuel assemblies, under accidental conditions (mrem/h)

Mantle	Lid	Bottom
16.6	< 29.5	< 76.3

Table 7-16b: Dose rates at a distance of 1 m of the TN 7-2 loaded with 2 RHF fuel assemblies, under accidental conditions (mrem/h)

Mantle	Lid	Bottom
47.4	< 27.3	< 59.3

7.7 Literature

/7-1/ TN 7/MTR Package Design, Safety Report,
TN report no. 7701

/7-2/ I. O. Blomeke/M. F. Todd:
U-235 Fission-Product Production as a Function of Thermal
Neutron Flux, Irradiation Time and Decay Time,
ORNL 2127, Oak Ridge

/7-3/ Safety Report, Transport of two Irradiated
RHF Fuel Assemblies in the TN 7 cask,
TN report no. 8021

/7-4/ T. Rockwell III:
Reactor Shielding Design Manual, Mc-Graw-Hill Book Company, Inc.
Princeton-New Jersey (1956)

/7-5/ K. H. Lindackers
Praktische Durchführung von Abschirmberechnungen,
Verlag Karl Thiemig KG, München (1962)

/7-6/ R. G. Jaeger:
Engineering Compendium on Radiation Shielding,
Vol. I, Springer Verlag, Berlin (1968)

/7-7/ IAEA-Regulations for the Safe Transport of Radioactive Materials, 1973

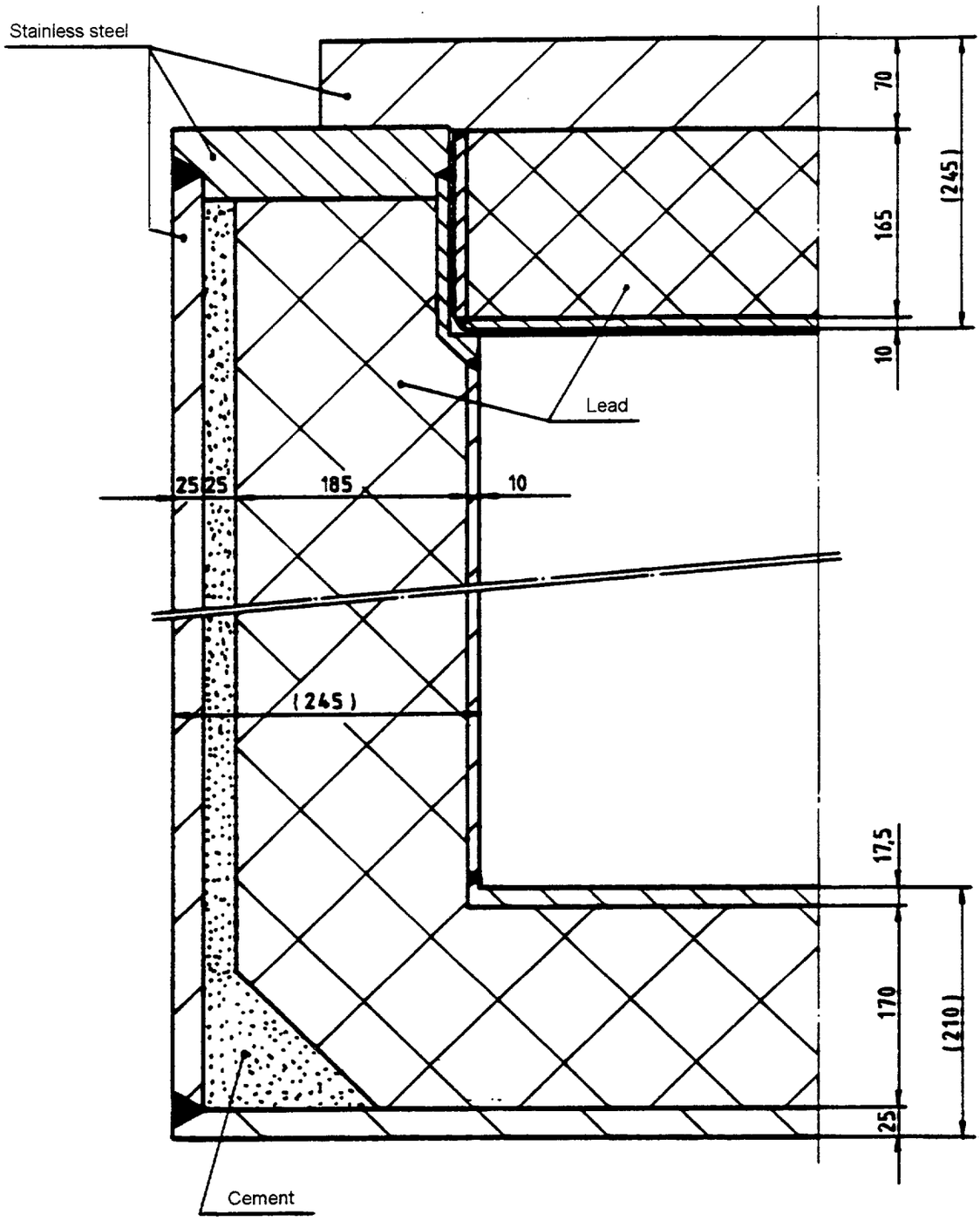

TN	Shielding thicknesses at mantle, lid and bottom of the TN 7-2	Fig. 7-1

× Receiving point

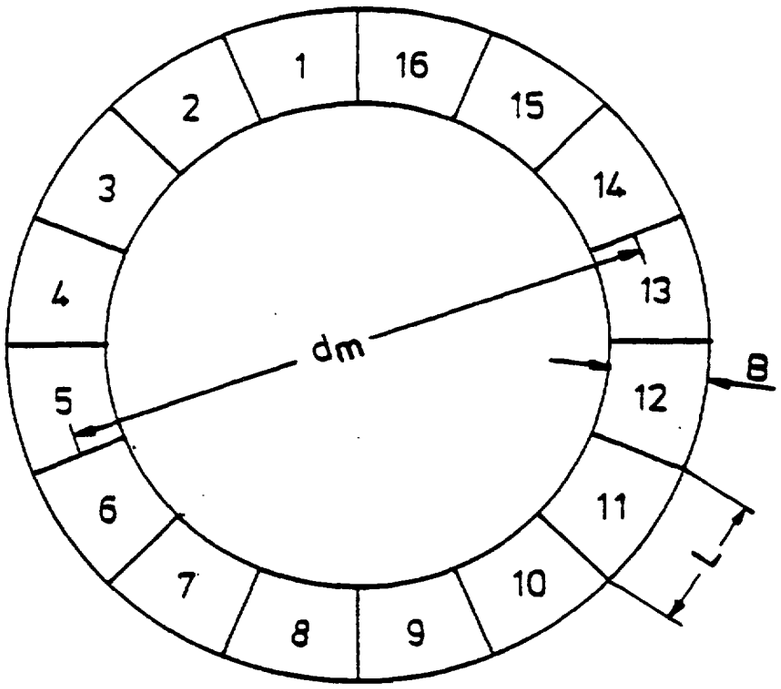

Subdivision of the RHF fuel assembly into linear sources

Fig. 7-2

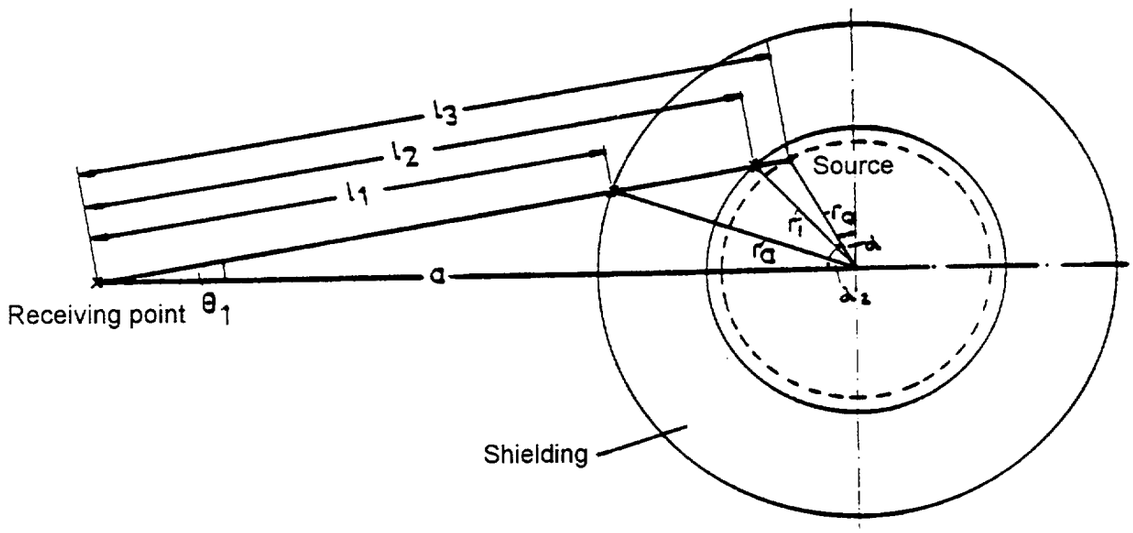

TNO	Geometry for the calculation of the mantle dose rate for RHF fuel assemblies	Fig. 7-3

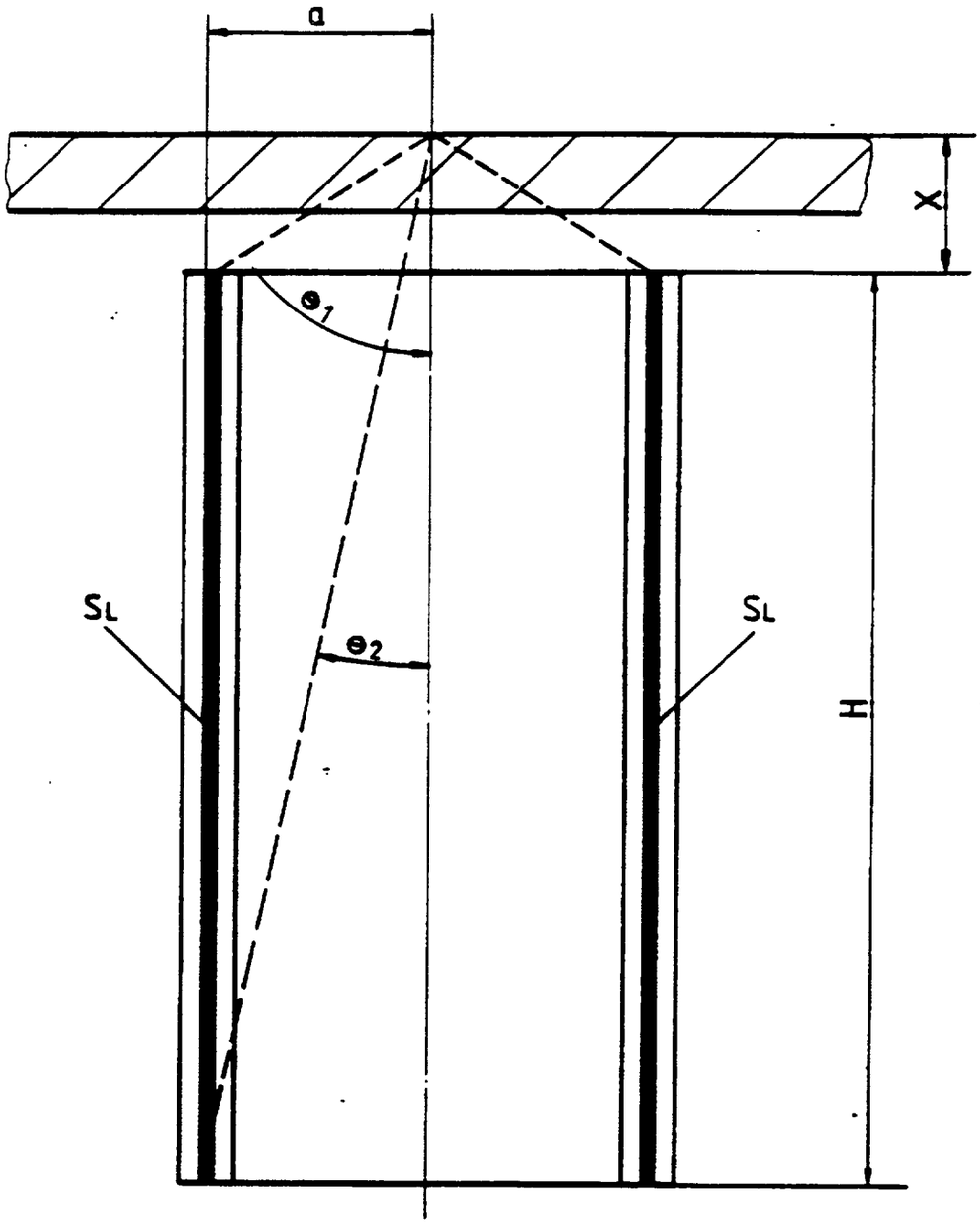

Model for the calculation of the dose rate at the front end, for RHF fuel assemblies

Fig. 7-4

8. Criticality safety

In the following it will be proven that the TN 7-2 flask, loaded with the various contents described in Chapter 2, satisfies the requirements for fissile class II packagings.

8.1 Fundamentals

The nuclear safety of the TN 7-2 flask is based upon the following factors:

- the fuel elements are as described in Chapter 2. The quantity of fissile material present in the unirradiated state will be used for calculation purposes.
- the body of the flask will retain its integrity and geometry even under accident conditions.
- the basket is so designed that its geometry will be retained under both normal and accident conditions.

8.2 Methods of proof

A. DIDO and MERLIN fuel elements

The baskets used for DIDO and MERLIN fuel elements are identical to those used in the TN 7. The usable inner diameter of the TN 7-2 is also the same as that of the TN 7 with additional shielding. The inner length, however, differs slightly between the two flasks. These differences are not important for the criticality safety analysis, as an infinitely long fuel zone is assumed.

A German package approval issued by the PTB (No. D/4001/B(U)F (Rev.0)) already exists for transporting these elements in the TN 7 (described in safety report /8-1/).

The differences to this package approval with respect to criticality safety are the following:

1. loading the flask with 2 DIDO and 2 MERLIN baskets is proposed, compared with max. 1 MERLIN basket in the TN 7.

2. changing the lateral construction of the flask, namely:

   - a different material layering sequence

   - varying total layer thicknesses of the individual materials (+ 0.5 cm lead, - 1.5 cm steel compared with the TN 7).

The first item has no effect on the criticality safety of the TN 7-2. This can be proven by the fact that the criticality safety analysis for the TN 7 flask assumed a longitudinally infinite fuel zone, both for DIDO and for MERLIN fuel elements. This showed that a load of solely DIDO fuel elements represents the most reactive state.

In spite of the different layering sequence mentioned in the second item, there is no change in reactivity to be expected as the thickness of the layers is practically identical.

Proof of criticality safety is therefore based on the following document:

- criticality safety of DIDO and MERLIN fuel elements in the TN 7 (H. Krug, University of Munich, 1976), annex to the TN 7 safety report (/8-1/).

This report is contained in Appendix 8.1.

B. RHF fuel elements

The basket used in the TN7-2 for 2 RHF fuel elements is identical to that used in the TN 7. As far as the varying packaging geometries of the TN 7 and TN 7-2 are concerned, the remarks made in section 8.2 A apply.

A German package approval for the TN 7 with these contents (described in /8-2/) has been applied for at the PTB.
The difference to this package approval lies, in reference to the criticality safety in the present case, in the change in packaging construction mentioned in section 8.2 A.

Proof of criticality safety is therefore based on the following document (see Appendix 8.2):

- criticality safety of irradiated RHF fuel elements in the TN 7 transport flask (W. Weber, H. Krug, GRS, 27.4.1982).

8.3 Results

B. RHF fuel elements

The results correspond to those calculated for the same loading in the TN 7 (see Appendix 8.2). The influence of the changed flask geometry is negligibly small.

The following values were recorded:

- 2 flooded flasks

  For a loading of 2 RHF fuel elements in each flask in the given transport state (see Chapter 2)

  $K_{eff} + \Delta K_{eff} = 0.946$ $\qquad$ $\Delta K_{eff} = 2\ \sigma$

  under full water reflection (30 cm water layer).

- collection of dry flasks

  Any number of dry flasks is sub-critical.

Thus the TN 7-2 flask, loaded with 2 RHF fuel elements, satisfies the criteria of the nuclear fissile class II.

8.4 References

/8-1/ TN 7 / MTR Package Design, Safety Report,
TN report no. 7701

/8-2/ Safety Report, Transport of 2 irradiated RHF fuel elements in the TN 7 flask,
TN report no. 8021

CRITICALITY SAFETY

OF DIDO AND MERLIN FUEL ELEMENTS

IN THE TN-7 CASK

(Translation)

Herwin Krug
University of Munich
December 1976

SUMMARY

Criticality safety for the transport of Dido and Merlin type MTR-elements in the container TN-7 was investigated. An insert with 15 transport positions out of steel tubes is foreseen for the round Dido fuel elements and an insert with 16 transport positions consisting of almost square steel boxes is foreseen for the box-shaped Merlin fuel elements. Up to four fully laden inserts are to be transported in the container TN-7, Dido and Merlin inserts being simultaneously present in the container.

It is shown that the most reactive situation occurs if the container is completely flooded. The effects of possible incidents - varying moderation of the fissile material and decreased water tightness - were investigated for this situation. It was established that the multiplication factor of the container is always below 0.9. When the container is dry, the multiplication factor is under 0.51.

The multiplication factors indicated refer to the flooded or dry state of containers lying close together in an infinitely vast arrangement. As a result the transport of Dido and Merlin fuel elements in the TN-7 with the inserts investigated has to be classified in the nuclear safety class II.

1.0 Introduction

2.0 Calculating method, general assumptions

3.0 Flooded container with DIDO fuel elements

3.1 Group constants for DIDO fuel elements

3.2 Group constants for DIDO basket lattice cells

3.3 DIDO inserts in the TN-7

4.0 Flooded container with MERLIN fuel elements

4.1 Group constants for MERLIN fuel elements

4.2 Group constants for MERLIN basket lattice cells

4.3 MERLIN inserts in the TN-7

5.0 DIDO and MERLIN inserts in the TN-7

6.0 Temperature influence

7.0 Dry container

8.0 Appendixes

9.0 References

10.0 Supplement

10.1 Boron steel basket for DIDO elements

10.2 Boron steel basket for MERLIN elements

1. Einführung

The task of investigating the criticality safety of the container TN-7 (Appendix 8.1) for the transport of round MTR fuel elements of the Dido type and of the box-shaped MTR fuel elements of the Merlin type was set. A separate insert is foreseen for each fuel element type. The layout of the inserts is restricted by the useful internal diameter of the TN-7, which is about 54 cm. Since the useful height of the TN-7 is 280 cm, as opposed to 60 cm active length of the fuel elements, up to four inserts can be transported on top of each other in the TN-7. Besides, the transport container should be loaded at one and the same time with inserts for the various fuel element types.

The Dido fuel elements consist of four concentrical rods, made of round, convex fuel plates (Appendix 8.2 and 8.3). The fuel plates themselves are composed of an uranium/aluminium core (layer thickness 0.066 cm) which is encased on both sides by an aluminium layer (0.0425 cm each). In all, a Dido fuel element contains 185 g U-235, with a degree of enrichment between 80 and 93 % and uranium core content of about 17-18 %. However, during transport the rods of the Dido fuel elements are not concentric; the rods in each fuel element are secured together at one side (Appendix 8.4).

The insert for the Dido fuel element contains 15 transport positions. The transport positions are in the form of steel rods with an internal diameter of 10.4 cm and a wall thickness of 0.5 cm. These rods are fixed in two concentric circles on an annular spacing structure (figure 1). However, it can be seen from the critical analysis of the Dido insert which follows, that these dimensions are of minor importance only.

Figure 1 : DIDO insert

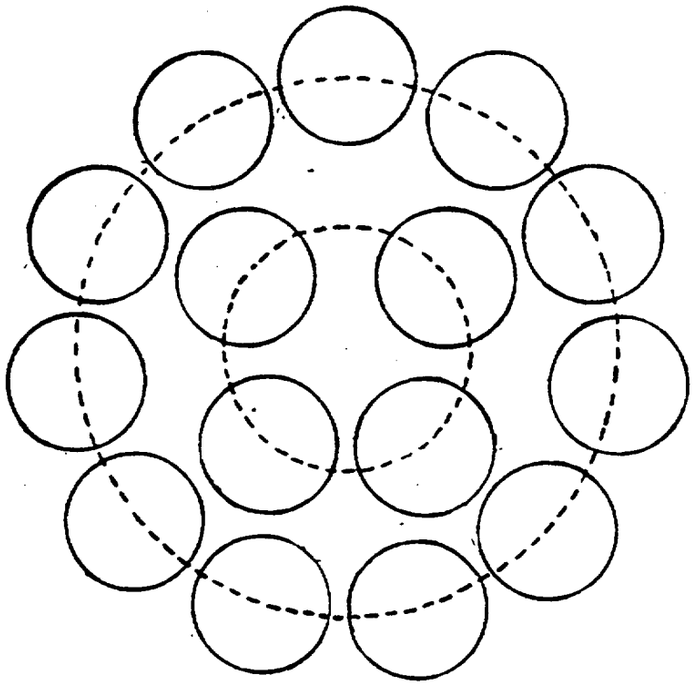

Figure 1 : MERLIN insert

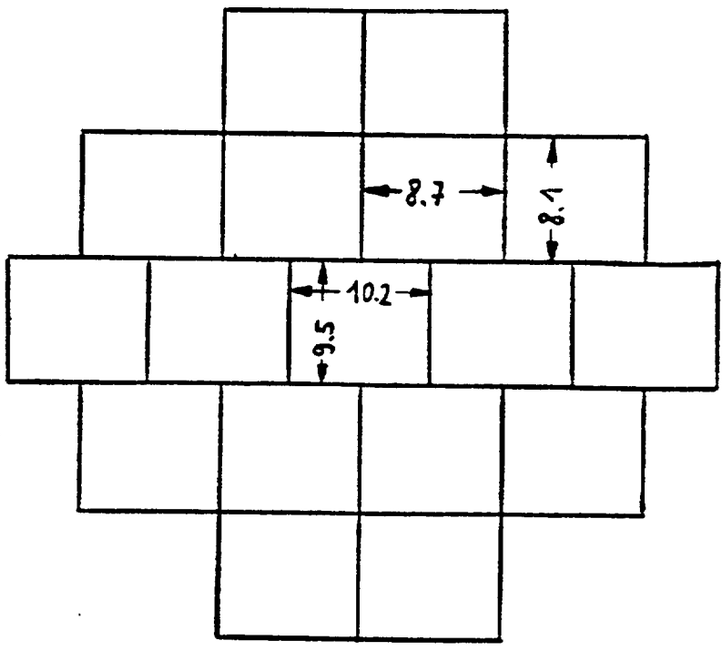

The Merlin fuel elements are an example of classical box-shaped MTR fuel elements with more or less square cross-section (Appendix 8.5, 8.6 and 8.7). The Merlin fuel elements contain 270 g U-235, likewise with a degree of enrichment between 80 and 93 %. The Merlin fuel plates themselves are composed of an uranium/aluminium core (layer thickness 0.051 cm), encased by an aluminium layer (0.038 cm each) on both sides. The uranium content in the core amounts to about 21 to 27 %.

The insert for the Merlin fuel elements contains 16 transport positions. The transport positions are in the form of almost square steel boxes lying close together (inner dimensions 8.7 cm x 8.1 cm) with a wall thickness of 0.7 cm. The relationship of the steel boxes to an insert is clearly visible from figure 2. Steel poisoning is foreseen neither for the Dido nor for the Merlin fuel element inserts.

In order to judge the criticality safety in the cases mentioned above, the container flooded state is of decisive importance, as the highest reactivity can be reached here. Consequently the following criticality analysis is primarily concerned with the flooded state. In addition, an arrangement of dry containers is also examined, as differing conditions can occur with respect to neutron interaction.

2. Calculating method - General assumptions

The method of calculation applied, which is particularly adapted to the flooded state of the container, can be divided into three main steps :

1. determination of the cross-sections for the active zones and structure materials
2. determination of homogenized cross-sections for the various basket lattice cells
3. determination of the loaded container with the various basket lattice cells.

This method of calculation, which suggests itself thanks to the arrangement of the transport positions in the inserts, has proved to be of particular value for the calculation of transport containers (Ref. 1 and 2). The group constants for fuel element areas and structural materials were calculated with the GAMTEC programme (Ref. 5). For the determination of fast group constants the B-1 approximation was used, for the determination of the thermal group constants of the fuel zones the Wigner-Wilkins approximation using water moderation and of structural materials a Maxwell distribution. These group constants all related to room temperature and a geometric buckling of 1.10^{-4}.

For the determination of nuclide densities the following values were uniformly applied: water, 1.0 g . cm^{-3}; lead, 10.77 g . cm^{-3} and for steel 7.566 g . cm^{-3} (composition according to DIN 1.4301 ≙ X5CrNi 189 ≙ SS - 304). The densities for lead and steel in the calculation are only 95 and 97 % respectively of the actual densities, in order to take density changes such as may occur through fabrication variations and thermal expansion conservatively into consideration.

The group constants, which are homogenized for the transport positions, were produced by the multi-group diffusion programme CITATION (Ref. 6). The container calculations were also carried out with the CITATION programme. A local flux convergence of 10^{-3} was asserted for all CITATION calculations. All calculations in the flooded state were carried out with four neutron groups. The four group standard set-up for light water reactors (10 MeV - 8.21 KeV - 5.53 KeV - 0.625 eV - 0.0 eV) was used as group classification.

For the criticality analysis of dry containers the Hansen-Roach cross-section for 16 neutron groups, especially devised for hard neutron spectra, was used (Ref. 3). Determination of the reactivity was carried out by the Monte-Carlo programme KENO (Ref. 7).

3. Flooded container with DIDO fuel elements

3.1 Group constants for DIDO fuel elements

As the degree of enrichment given for DIDO fuel elements was only between 80 and 93 %, it was conservatively assumed that the entire uranium was present in the form of U-235, in order to cover the whole range of enrichment. In particular a uranium quantity of 200 g U-235 per fuel element was taken as a basis. Assuming a full material density for U-235 ($g = 18.662\ g \cdot cm^{-3}$) and for aluminium ($g = 2.698\ g \cdot cm^{-3}$) the uranium content in the core was calculated at 17.738 %. This results in the following nuclide densities:

1)	Core	U-235	$= 0.14459 \cdot 10^{-2}\ b^{-1} \cdot cm^{-1}$
		Al	$= 0.58401 \cdot 10^{-1}\ b^{-1} \cdot cm^{-1}$
2)	Al-cladding	Al	$= 0.60222 \cdot 10^{-1}\ b^{-1} \cdot cm^{-1}$

Fluctuations in the uranium content in the core are only noticeable with a constant uranium quantity (200 g) in the nuclide density for aluminium. Minor fluctuations in the nuclide density of aluminium are caused by insignificant reactivity changes in the fuel elements, as was shown in an experiment on MERLIN fuel plates of similar structure, described in section 4.1.

For further calculations, the fuel plates were homogenized with the surrounding water, an approach which led to conservative results with highly enriched uranium. For this homogenization only the active part of the fuel plates was used. Since no clear-cut volume or fixed water or moderator percentages can be attributed to the DIDO fuel elements in a transport position because of the layout of the fuel rods

(Appendix 8.4), a series of calculations was carried out, in which areas of transport positions of varying sizes were homogenized. In Table 1 those measurements, resulting from these calculations, are listed which enable an easy assessment of the reactivity of the fuel elements with varying homogenization volumes.

Table 1

% Vol	R /cm/	K_∞	B_m^2	τ	L^2	p	$\eta\epsilon_1$	$\eta\epsilon_2$
100	5.2	1.5623	.0156	31.799	2.9602	.95581	1.2232	1.578
90	4.9332	1.6008	.0164	32.553	2.8431	.95126	1.2545	1.618
80	4.6510	1.6408	.0170	33.541	2.7272	.94534	1.2874	1.661
70	4.3506	1.6820	.0175	34.899	2.6167	.93731	1.3221	1.706
65	4.1924	1.7030	.01769	35.786	2.5659	.93212	1.3401	1.729
60	4.0279	1.7240	.01775	36.875	2.5207	.92580	1.3586	1.753
55	3.8564	1.7450	.01768	38.246	2.4828	.91796	1.3775	1.777
50	3.6770	1.7656	.0174	40.021	2.4591	.90795	1.3970	1.803
40	3.2888	1.8033	.0162	45.802	2.4874	.87646	1.4373	1.854

In the first column the percentual volume of the transport position is given, on which the homogenization was based. 100 % implies homogenization of the whole transport position or of the whole available internal surface of a rod in the insert. In column 2 the corresponding equivalent radius of the fuel element volume with an active height of 60 cm is given.

3.2 Group constants for DIDO basket lattice cells

From Table 1 it cannot be seen which fuel element data give the most reactive group constants for the basket lattice cell. This is due to the fact that neither the reactivity effect on the water particles remaining in the basket lattice cell nor the reactivity effect of neutron absorption in the steel tube of the transport position can be estimated because of the internal neutron flux. Consequently group constants for the corresponding basket lattice cells were calculated for all fuel element data. In the calculating model the basket lattice cell was described as a cylindrical fuel element zone with radius R_{BE}, a water ring zone of ΔR_{H_2O} and steel tube transport position (0.5 cm). As limiting condition full reflection ($\nabla \Phi = 0$) was assumed on the outer surface of the tube. This assumption leads to conservative results as will be shown later in this chapter.

Table 2

% Vol	R_{BE}	ΔR_{H2O}	K	B^2_M	τ	L^2
100	5.2	0.0	1.1209	.00321	35.096	2.544
90	4.9332	0.2668	1.1131	.00301	35.093	2.528
80	4.6510	0.5490	1.0946	.00251	35.106	2.531
70	4.3506	0.8494	1.0645	.00171	35.146	2.558
65	4.1924	1.0076	1.0449	.00119	35.180	2.584
60	4.0279	1.1721	1.0217	.00057	35.226	2.619
55	3.8564	1.3436	.9949	÷00013	35.288	2.665
50	3.6770	1.5230	.9639	÷00095	35.371	2.726
40	3.2888	1.9112	.8874	÷00292	35.629	2.907

Table 2 shows that the most reactive group constants for the basket lattice cells occur throughout the entire transport position during homogenization.

The most reactive group constants for the active zone with regard to material buckling occur in an active zone composed of 60 % volume of the transport position (table 1). It was therefore investigated whether in this case a more reactive basket cell is formed with an other than cylindrical fuel arrangement in the transport position. The calculating model for this is different from the previous one, in so far as the fuel is assumed to be in a circle in the basket lattice cell. The central water volume was increased from 0 to 40 % volume of the transport position, i.e. until the active zone inside finally touches the tube lining of the transport position. The results are given in table 3.

Table 3

% Vol	R_{H2O}	ΔR_{BE}	ΔR_{H2O}	K_∞
0	0.0	4.0279	1.1721	1.0217
5	1.1628	3.0295	1.0077	1.0456
10	1.6444	2.7062	0.8494	1.0582
20	2.3255	2.3255	0.5490	1.0589
30	2.8482	2.0849	0.2669	1.0335
40	3.2888	1.9112	0.0	0.9861

In the first column the central water volume is given as a percentage volume of the transport position. In the following columns the radius of the central water volume, as well as the thickness of the corresponding circular active and water zones respectively is given in cm. It can be seen from table 3 that the multiplication factor for a central water volume of about 20 % reaches a maximum. The reactivity of the basket lattice cell, even in this case, is well below the value obtained by homogenizing the fuel element over the whole transport position (table 2). For future experiments, it will always be assumed that the fuel element is homogenized for the whole transport position.

In the calculations made to date, an outer water layer in the basket lattice cells was not taken into account. Consequently a whole series of calculations was made, for which the basket lattice cell was extended by an outer circular layer of water. For this, the water layer varied between 0 and 2.0 cm.

The results are given in table 4.

Table 4

R_{H2O}	R_{Cell}	K_∞	B^2_M	τ	L^2
0.0	5.7	1.1209	.00321	35.096	2.544
0.1	5.8	1.0969	.00260	34.655	2.557
0.2	5.9	1.0740	.00201	34.251	2.576
0.285	5.985	1.0554	.00152	33.934	2.596
0.5	6.2	1.0111	.00031	33.223	2.664
1.0	6.7	0.9191	-.00232	31.962	2.904
1.271	6.971	0.8739	-.00365	31.447	3.069
2.0	7.7	0.7652	-.00690	30.445	3.582

In the first column the thickness of the outer water layer is given, and in the second column the resulting cell radius. It can be seen from table 4 that the reactivity of the basket lattice cell decreases sharply as the outer water layer increases. Mention should be made of two further examples which are apparent from table 4. An outer water layer of 0.285 cm corresponding to the case where all transport positions lie close together in a hexagonal lattice, i.e. there is the smallest possible lattice pitch. An outer water layer of 1.271 cm corresponds to a basket lattice cell resulting from a uniform distribution of the transport positions in the transport container. This case is the closest to the conditions which actually prevail.

3.3 DIDO inserts in the TN-7

The determination of the TN-7 reactivity was not based on a definite number of inserts, an infinite extension of the container with insert and fuel elements in an axial direction was conservatively assumed. The radial structure of the TN-7 is illustrated in Appendix 6.1.

In the calculation the radial structure was described by layers of steel (1 cm), lead (5 cm), steel (2 cm), lead (13 cm), steel (2 cm), lying close together, with a free internal radius of 27 cm.

The insert with the fuel elements was represented by a co-axial cylindrical zone, whose cross-section is equal to the surface area of all the basket lattice cells. The multiplication factor for the basket lattice cells of varying sizes, which differed only in their outer water layer (table 4), was calculated, assuming full reflection ($\nabla \Phi = 0$) as limiting condition on the outer wall of the container. This limiting condition gives conservative results, as will be shown in this chapter. The results of this calculation are given in table 5. In the first column is the cell radius, R_{cell} of the basket lattice cell which forms the insert; in the second column is the equivalent insert radius R_{insert} and in the 3rd column, in cm, the water layer thickness ΔR_{H2O} between the insert and the inner wall of the container.

Table 5

R_{Cell}	R_{Basket}	ΔR_{H2O}	K_∞
5.7	22.076	4.924	0.8980
5.8	22.463	4.538	0.8884
5.9	22.851	4.149	0.8791
5.985	23.180	3.820	0.8715
6.2	24.012	2.988	0.8532
6.7	25.949	1.051	0.8136
6.971	27.0	0.0	0.7896

It can be seen from table 5 that the container reactivity decreases sharply as the size of the basket lattice cells increase, i.e. with increasing outer water layer around the transport position. K_∞ values for basket lattice cells with a radius of less than 5.985 cm are of purely mathematical significance since - as already mentioned - the smallest possible distance between the steel tubes forming the transport positions would be surpassed.

The multiplication factors in table 5 are based on full neutron reflection on the outer container wall. Consequently the reactivity influence of an outer water layer was investigated. For this purpose the container calculating model was extended outside by an adjacent circular layer of water. This water layer ΔR_{H2O} was varied between 0 and 30 cm. Full reflection was again assumed as limiting condition. The basket lattice cell with radius of 5.985 cm or insert with equivalent radius of 23.18 cm respectively table 5) was conservatively taken for these calculations. The results can be seen in table 6.

Table 6

ΔR_{H2O}	0.0	1.0	2.0	4.0	8.0	15.0	30.0
K_∞	0.8715	0.8603	0.8581	0.8567	0.8563	0.8563	0.85

From this table it can be seen that the reactivity drops as the outer water layer thickness increases, i.e. that the assumption of full reflection on the outer container wall leads to conservative results. From the very slight decrease in K_∞ it can be concluded that TN-7 containers are almost completely neutralized against each other as far as neutrons are concerned, thanks to the container structure.

4. Flooded container with MERLIN fuel elements

4.1 Group constants for MERLIN fuel elements

Analogous with DIDO fuel elements, it was likewise assumed for MERLIN fuel elements that the entire uranium was present in the form of U-235. In particular, a basic uranium quantity of 290 g U-235 per fuel element was taken. Because of the high fluctuation of the aluminium content in the core, the reactivity effect of the aluminium in the core was investigated for uranium core contents of 21, 22, 25 and 30 %. With a constant uranium content of 290 g U-235 the corresponding aluminium values can be calculated. When one compares these values with the total active volume of the fuel plates, the following nuclide densities result in the core :

U-235	$= 0.17524 \cdot 10^{-2}$	$b^{-1} \cdot cm^{-1}$
Al (U = 21 %)	$= 0.58066 \cdot 10^{-1}$	"
Al (U = 22 %)	$= 0.54112 \cdot 10^{-1}$	"
Al (U = 25 %)	$= 0.45787 \cdot 10^{-1}$	"
Al (U = 30 %)	$= 0.35612 \cdot 10^{-1}$	"

The same aluminium thickness as for DIDO fuel plates was assumed for the cladding.

For the determination, the fuel plates were homogenized similarly to the DIDO fuel plates. Contrary to the DIDO fuel element, a definite homogenization volume can be attributed to the MERLIN fuel element due to the constant lattice pitch of 0.342 cm. However, with regard to incidents such as compaction of the fuel plates or increase in the lattice pitch through dislocation, the reactivity effect caused by alteration of the lattice pitch or the

homogenized volume respectively was examined closely. In particular, a lattic pitch of 0.171 cm corresponding to an effective fuel element expanse of 6.3 x 3.76 cm^2, if fuel plate compaction occurred, was considered. Should expansion occur, fuel element expanses of 7.56 x 7.56 cm^2, 7.96 x 7.96 cm^2 and 8.7 x 8.1 cm^2 were investigated. With regard to the homogenization of the fuel plates, this corresponds to effective lattice pitches of 0.413 cm, 0.458 cm and 0.508 cm. Characteristic reactivity values for these calculations are given in table 7. It can be seen from this table that a uranium content of ca. 21 % in the core gives the most reactive values with reference to material buckling, whereas if the uranium content increases the rise in the multiplication factor is negligible. As a result, only group constants with a uranium content of 21 % in the core are used for the basket lattice calculations.

Table 7

BE	%U-235	K_∞	B^2_m	τ	L^2	P	$(\eta f)_1$	$(\eta f)_2$
0.171_a	21%	1.7743	0.0067	111.68	4.0919	0.57188	1.5264	1.9599
23.701_b	22%	1.7761	0.0066	113.63	4.1116	0.57200	1.5282	1.9615
$33.63\%_c$	25%	1.7798	0.0064	118.00	4.1535	0.57225	1.5320	1.9650
$6.3x3.76_d$	30%	1.7843	0.0061	123.84	4.2049	0.57255	1.5366	1.9692
0.342_a	21	1.8091	0.0171	43.626	2.3038	0.87726	1.4426	1.8604
47.401_b	22	1.8105	0.0170	44.000	2.3069	0.87734	1.4440	1.8618
$67.26\%_c$	25	1.8135	0.0168	44.812	2.3138	0.87750	1.4468	1.8647
$6.3x7.52_d$	30	1.8172	0.0165	45.848	2.3229	0.87770	1.4503	1.8683
0.413_a	21	1.7791	0.0182	39.289	2.3038	0.90361	1.4099	1.8185
57.229_b	22	1.7804	0.0181	39.568	2.3067	0.90368	1.4112	1.8198
$81.21\%_c$	25	1.7833	0.0179	40.168	2.3125	0.90381	1.4139	1.8226
$7.56x7.56_d$	30	1.7868	0.0176	40.929	2.3200	0.90397	1.4171	1.8260
0.458_a	21	1.7584	0.0184	37.515	2.3347	0.91473	1.3900	1.7923
63.423_b	22	1.7597	0.0183	37.755	2.3380	0.91478	1.3912	1.7947
$90.00\%_c$	25	1.7625	0.0182	38.270	2.3433	0.91490	1.3938	1.7963
$7.96x7.96_d$	30	1.7659	0.0180	38.920	2.3500	0.91505	1.3969	1.8000
0.508_a	21	1.7343	0.0185	36.003	2.3852	0.92435	1.3679	1.7643
70.47_b	22	1.7356	0.0184	36.210	2.3877	0.92440	1.3691	1.7656
$100\%_c$	25	1.7383	0.0183	36.653	2.3929	0.92451	1.3715	1.7683
$8.7x8.1_d$	30	1.7415	0.0181	37.211	2.3990	0.92464	1.3746	1.7717

a : lattice pitch
b : fuel element surface
c : % volume fuel element to transport position
d : fuel element dimensions in cm

4.2 Group constants for MERLIN basket lattice cells

In accordance with the construction of the insert (fig. 2) the almost square transport position box was considered as basket lattice cell (fig. 3) and the limiting condition of full reflection ($\nabla \Phi = 0$) was assumed. Furthermore, a centrical location for the fuel element was supposed. Due to the resulting symmetry, the calculating model could be restricted to a quarter representation of the basket lattice cell. The reciprocal transfer of the transport positions was not taken into consideration in this calculating model. However, it is shown in Ref. 1 that reciprocal transfer has practically no effect on the group constants.

Figure 3

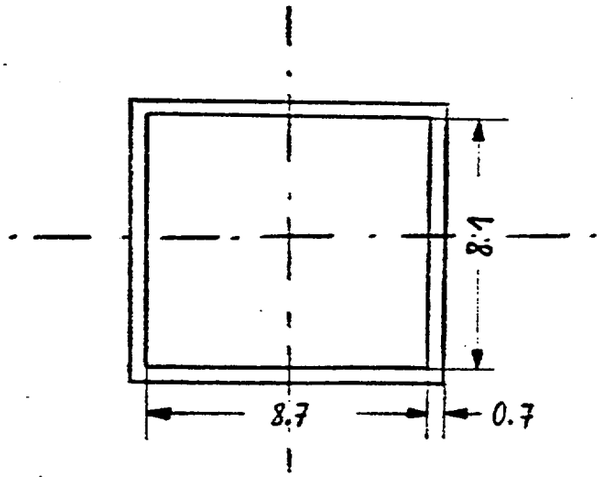

The assumption of full reflection on the outside should be judged conservatively as each transport position has water on at least one side. This was established from the calculations previously made for DIDO fuel elements. For the active zones which deviate sharply from a square cross-section (6.3 x 3.76 cm^2 and 6.3 x 7.52 cm^2) both possible positions in a centrical arrangement in the transport position were examined.

The calculating models for the fuel elements of various dimensions and the results are assembled in figure 4. In cases 1 and 2, the broken lines indicate the possible alternative positions; the corresponding results are given in brackets. It can be seen from figure 4 that the most reactive group constants occur throughout the whole transport position when the fuel element is homogenized, whereas the reactivity of the basket lattice cell diminishes as the fuel element cross-section or homogenized volume respectively decreases. This implies that compacted fuel elements lead to lower multiplication factors.

As already mentioned, a centrical location for the fuel element was always supposed in the transport position. However, an excentrical location of the fuel element does not generally increase the reactivity (Ref. 1). This is due to the fact that the negative reactivity effect from the increase in the water column between the fuel element and the basket wall outweighs the positive reactivity effect from the reduction in the water column on the opposite side of the fuel element. This effect can be seen equally well from fig. 4, cases 1 and 2. The fuel elements drawn in broken lines lie with one side nearer to the basket wall and therefore result in less reactive basket lattice cells.

4.3 MERLIN inserts in the TN-7

Analogous to the DIDO inserts, an infinite extent of MERLIN inserts with fuel elements and of the container was assumed here, in axial direction. The radial container structure was retained (chapter 3.3). Full reflection ($\nabla \Phi = 0$) was assumed on the outer wall of the container. The conservativity of this assumption was already pointed out in chapter 3.4.

Figure 4

1. Fuel element 6.3 x 3.76 cm^2

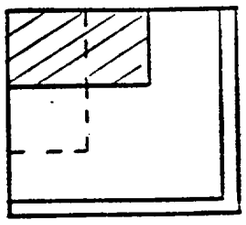

K_{∞} = 0.7836 (0.7710)

M^2 = 48.439 (48.580)

B_m^2 = -.0045 (-.0047)

2. Fuel element 6.3 x 7.52 cm^2

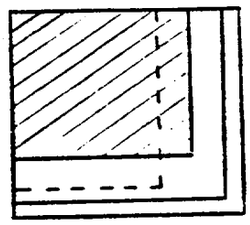

K_{∞} = 1.0990 (1.0866)

M^2 = 45.050 (45.039)

B_m^2 = 0.0022 (0.0019)

3. Fuel element 7.56 x 7.56 cm^2

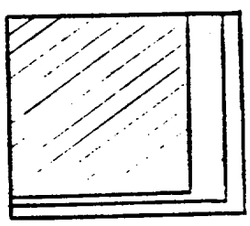

K_{∞} = 1.1626

M^2 = 44.675

B_m^2 = 0.0036

4. Fuel element 7.96 x 7.96 cm^2

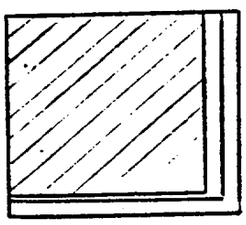

K_{∞} = 1.1890

M^2 = 44.669

B_m^2 = 0.0042

5. Fuel element 8.7 x 8.1 cm^2

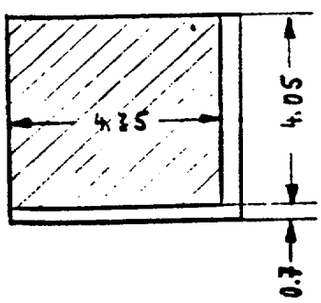

K_{∞} = 1.2095

M^2 = 44.617

B_m^2 = 0.0047

The insert was represented as a co-axial circular zone in the container, corresponding to its construction (fig. 2) for the calculation. The inner radius of this zone results from the radius of the cylinder which has an equal surface area to the central water hole (R_i = 5.56 cm). The outer radius is determined by analogy with the surface area of the 16 basket cells (R_a = 22.79). This cylindrisation leads to conservative results, since the surface to volume ratio and subsequently the neutron leakage in the surrounding water is reduced (Ref. 1). The multiplication factor of the container was calculated for each basket lattice cell illustrated in fig. 4. The results are given in table 8.

Table 8

BE	6.3 x 3.76	6.3 x 7.52	7.56 x 7.56	7.96 x 7.96	8.7 x 8.
K_B	0.5765 (0.5662)	0.8241 (0.8138)	0.8732	0.8930	0.9078

The multiplication factors in brackets correspond once again to the alternative fuel element locations in the transport positions. As the MERLIN fuel element, contrary to the DIDO fuel element, can be attributed with a fixed cross-section of 6.3 x 7.52, a multiplication factor of 0,8241 should be applied in this instance in order to judge the criticality safety. Compaction of the fuel element causes a sharp reduction, and expansion of the fuel element an increase, in the container multiplication. At any rate, the case with a fuel element dimension of 8.7 x 8.1 cm^2 is more of mathematical significance, as in practice it can never arise. Considering the accumulation of conservativities, the actual multiplication factor in this case will also be below 0.9.

Furthermore, the reactivity effect of manufacturing tolerances for the MERLIN insert in the container was investigated. The surface cross-section of the central water hole ($F = 97.09\ cm^2$) was taken as parameter. An average reactivity coefficient $K_B^{-1} \cdot \Delta K_B / \Delta F = -3.8 \cdot 10^{-4}$ resulted uniformly throughout the container with the various basket lattice cells (fig. 4). Diminishing of the central water hole increases, and increasing of the central water hole therefore reduces, the container multiplication. Because this reactivity coefficient is so low, this effect is not of importance for criticality safety with the normal fabrication variations.

5. DIDO and MERLIN inserts in the TN-7

Loading of the TN-7 simultaneously with DIDO and MERLIN inserts presents no particular criticality safety problem. The multiplication factor lies between those for the container when fully laden with DIDO or MERLIN inserts respectively. This is due to the fact that neutrons from the more reactive zone diffuse to the less reactive zone. To illustrate this point another sample calculation was performed. The calculating model for this is generally of cylindrical geometry and is illustrated in fig. 5. For the calculating model an infinite range of alternate DIDO and MERLIN inserts in axial direction was taken.

Figure 5

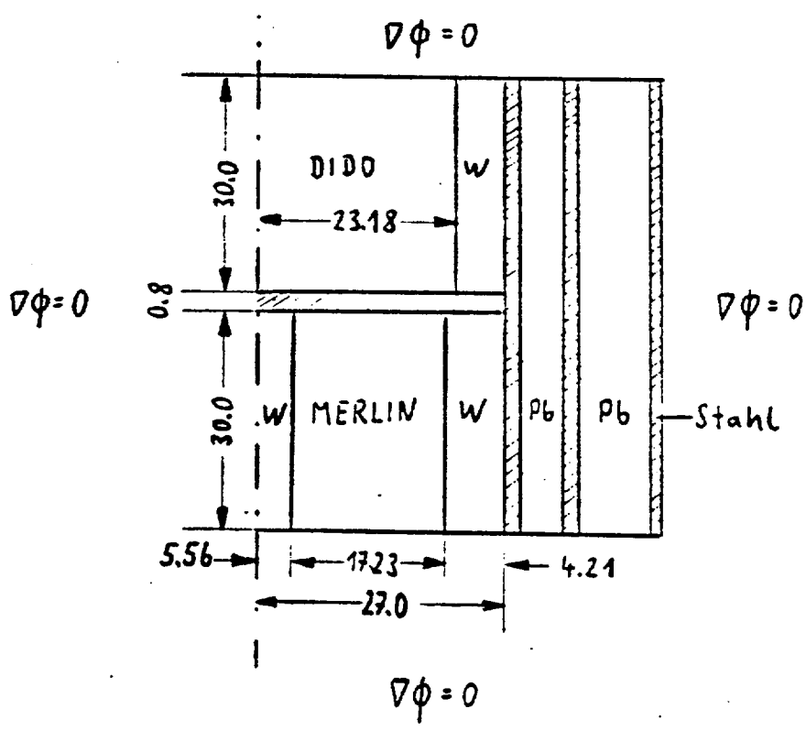

Between the inserts, as provided for in practice, a steel plate (0.8 cm thick) was taken into account. The actual container structure was retained. The DIDO insert corresponds to the case of rods lying close together after homogenization of the fuel elements throughout the transport position. The MERLIN insert corresponds to the basket lattice, case 2 in figure 4. A multiplication factor of 0.8402, i.e. between the values for the DIDO insert (0.8715) and for the MERLIN insert (0.8241) was determined for this arrangement.

6. Temperature influence

The experiments were carried out up till now at room temperature. In principle, higher temperatures are only noticeable with the available fissile material systems through a reduction in density, due to the thermal expansion on the reactivity. In the flooded state, the water density is the decisive element for reactivity. Consequently, the case of reduced water density was investigated for both fuel element and basket types. In particular, water densities of 0.9 and 0.8 g · cm^{-3} in the respective active zones were taken. The geometrical dimensions were retained unchanged, so that the uranium and aluminium densities remained the same.

For the DIDO fuel elements group constants corresponding to the assumptions presented in chapter 3.1 for both reduced water densities were calculated again. The most important characteristic criticality measurements, deduced from these calculations, are given in table 9. From table 9 it can be seen that the K_∞ increases with decreasing water density, but that the material buckling also decreases. This is due to the fact that the increase in the migration area M^2 is more noticeable for material buckling.

Which effect in the end has the greatest influence on the container multiplication factor can only be established by further calculations. As a result, more group constants for the DIDO basket lattice cells similar to those shown in chapter 3.2, table 2 were calculated. For this, the water density in the active zone was reduced, whilst the water density in the ring between the active zone and the steel rod of the transport position was conservatively retained. The characteristic criticality measurements resulting from these calculations are given in table 10. From table 10 it can be seen that the

Table 9

% Vol	ρ-H_2O	K_∞	B_m^2	τ	L^2	M^2
100	1.0	1.5623	.0156	31.799	2.960	34.759
	0.9	1.5946	.0136	38.644	3.411	42.055
	0.8	1.6279	.0116	47.975	3.995	51.970
90	1.0	1.6008	.0164	32.553	2.843	35.396
	0.9	1.6303	.0142	39.491	3.275	42.766
	0.8	1.6605	.0121	48.920	3.831	52.751
80	1.0	1.6408	.0170	33.541	2.727	36.268
	0.9	1.6671	.0147	40.601	3.137	43.738
	0.8	1.6938	.0124	50.166	3.670	53.836
70	1.0	1.6820	.0175	34.899	2.617	37.516
	0.9	1.7047	.0151	42.125	3.009	45.134
	0.8	1.7275	.0127	51.870	3.517	55.387
65	1.0	1.7030	.0177	35.786	2.566	38.352
	0.9	1.7237	.0152	43.122	2.950	46.072
	0.8	1.7443	.0127	52.986	3.447	56.433
60	1.0	1.7240	.0177	36.875	2.521	39.396
	0.9	1.7426	.0152	44.344	2.896	47.240
	0.8	1.7608	.0127	54.357	3.384	57.741
55	1.0	1.7450	.0177	38.246	2.483	40.729
	0.9	1.7612	.0151	45.881	2.854	48.735
	0.8	1.7769	.0127	56.086	3.335	59.421
50	1.0	1.7656	.0174	40.021	2.459	42.480
	0.9	1.7792	.0149	47.870	2.825	50.695
	0.8	1.7921	.0125	58.318	3.300	61.618
40	1.0	1.8033	.0162	45.802	2.487	48.289
	0.9	1.8109	.0138	54.348	2.857	57.205
	0.8	1.8174	.0116	65.602	3.332	68.934

Table 10

% Vol	$\rho - H_2O$	K_∞	B_m^2	τ	L^2	M^2
100	1.0	1.1209	.00321	35.096	2.544	37.640
	0.9	1.1259	.00281	41.967	2.844	44.811
	0.8	1.1290	.00237	51.090	3.222	54.312
90	1.0	1.1131	.00301	35.093	2.528	37.621
	0.9	1.1149	.00261	41.172	2.809	43.981
	0.8	1.1150	.00221	48.907	3.161	52.068
80	1.0	1.0946	.00251	35.106	2.531	37.637
	0.9	1.0931	.00216	40.287	2.790	43.077
	0.8	1.0895	.00179	46.883	3.116	49.999
70	1.0	1.0645	.00171	35.146	2.558	37.704
	0.9	1.0598	.00141	39.549	2.796	42.345
	0.8	1.0529	.00110	45.007	3.094	48.101
65	1.0	1.0449	.00119	35.180	2.584	37.764
	0.9	1.0384	.00091	39.203	2.811	42.014
	0.8	1.0303	.00064	44.125	3.094	47.219
60	1.0	1.0217	.00057	35.226	2.619	37.845
	0.9	1.0140	.00034	38.873	2.835	41.708
	0.8	1.0046	.00010	43.278	3.104	46.382
55	1.0	.9949	-.00013	35.288	2.665	37.953
	0.9	.9860	-.00034	38.563	2.871	41.434
	0.8	.9756	-.00053	42.469	3.127	45.596
50	1.0	.9639	-.00095	35.371	2.726	38.097
	o.9	.9542	-.00111	38.277	2.921	41.198
	0.8	.9431	-.00127	41.697	3.163	44.860
40	1.0	.8874	-.00292	35.629	2.907	38.536
	0.9	.8768	-.00301	37.800	3.083	40.883
	0.8	.8652	-.00309	40.287	3.301	43.588

migration area increases with the decrease in the water density and therefore material buckling drops, whilst there is no significant increase of K_∞ if the fuel element is homogenized over 100 or 90 % respectively of the transport position. However, because of the sharp increase of the migration area, the container multiplication factor will in any case drop with decreasing water density. This fact was verified by complete container calculations for the most reactive basket lattice cell (homogenization of the fuel element over the whole transport position, cell radius 5.7 cm, basket radius 22.076 cm). The exact calculating model is given in chapter 3.3. The results of these calculations are to be found in table 11.

Table 11

ϱ-H_2O	1.0	0.9	0.8
K_β	0.8980	0.8787	0.8541

Similarly, group constants for the various fuel element sizes, as described in chapter 4.1, were calculated with water densities of 0.9 and 0.8 g · cm^{-3}. The uranium content in the core was 21 %. The characteristic criticality measurements from these calculations are given in table 12. It can be seen from table 12 that the reactivity rates for the MERLIN fuel elements are similar to those for the DIDO fuel elements (table 9). Consequently, no calculations were made for group constants for MERLIN basket lattice cells with reduced water densities. When comparing a MERLIN basket lattice cell with the most reactive DIDO basket lattice cell (without external water layer), then the proportion of steel is 30 % higher for a MERLIN basket lattice cell than for a DIDI basket lattice cell. As a result,

the reactivity absorption for MERLIN basket lattice cells is greater with reduced water density.

Table 12

BE-WEITE	ϱ-H_2O	K_∞	B_m^2	τ	L^2	M^2
6.3x3.76	1.0	1.7743	.0067	111.68	4.092	115.77
	0.9	1.7631	.0058	127.46	4.573	132.03
	0.8	1.7499	.0049	147.28	4.925	152.20
6.3x7.52	1.0	1.8091	.0171	43.626	2.304	45.930
	0.9	1.8169	.0146	51.891	2.646	54.537
	0.8	1.8236	.0122	62.815	3.090	65.905
7.56x7.56	1.0	1.7791	.0182	39.289	2.304	41.593
	0.9	1.7918	.0155	47.039	2.648	49.687
	0.8	1.8037	.0129	57.363	3.094	60.457
7.96x7.96	1.0	1.7584	.0184	37.515	2.335	39.850
	0.9	1.7738	.0157	45.050	2.684	47.734
	0.8	1.7886	.0131	55.135	3.136	58.271
8.7x8.1	1.0	1.7343	.0185	36.003	2.385	38.388
	0.9	1.7525	.0158	43.355	2.742	46.097
	0.8	1.7703	.0132	53.236	3.204	56.440

7. Dry container

When investigating the criticality safety of the dry container only the MERLIN fuel elements need be taken into consideration as these have the highest fissile material content. In all, 18.56 kg U-235 can be found in the TN-7 with four fully laden inserts. The volume percent of fissile material in the active part of a fuel plate amounts to ca. 0.015. The critical, unreflected spherical mass of U-235 at such a dilution in aluminium is ca. 1400 kg U-235 (Lit. 4), so that no criticality problem is to be expected for the dry container.

Because of the container reflection on the one hand and a neutron interaction with other containers on the other hand, two Monte-Carlo calculations were performed for an infinite expanse of square lattices composed of containers lying close together. For this the radial container structure was retained and infinite extent in an axial direction assumed. In case 1, the active part of the fuel plates was compacted to a cylinder in coaxial location (R = 9.47 cm). In case 2, it was assumed to be homogeneously distributed over the container interior. The actual basket material was always disregarded. In both cases a multiplication factor of ca. 0.51 resulted for the arrangement, so that even in a dry state any container arrangement is critically safe. This result was also to be expected from the experiments described in chapter 6.

8.0 Appendix

8.1 Container TN-7

8.2 DIDO fuel element

8.3 DIDO fuel plates

8.4 DIDO fuel element rods during transport

8.5 MERLIN fuel element cross-section

8.6 MERLIN fuel element, inner fuel plate

8.7 MERLIN fuel element, outer fuel plate

9. References

/1/ Criticality study of transport containers for irradiated fuel elements of the light water type
TN, Sept. 74, H. Krug

/2/ Criticality safety of a "Dry transport container" for irradiated fuel elements of the light water type, depending on the enrichment
TN, April 75, H. Krug

/3/ Los Alamos Group-Averaged Cross-Sections
LAMS-2941, Hansen, Roach et al.

/4/ Handbook of Nuclear Safety
DP-532, Jan. 61, H.K. Clark

/5/ GAMTEC II : A Code for Generating Consistent Multigroup Constants Utilized in Diffusion and Transport Theory Calculations
BNWL - 35, March 1965
Carter, Richey, Hughey

/6/ Nuclear Reactor Core Analysis Code : CITATION
ORNL - TM - 2496, Rev. 2, 1971
Fowler, Vondy, Cunningham

/7/ KENO - A Multigroup Monte Carlo Criticality Program
CTC - 5, September 1969

10. Supplement

10.1 Boron steel basket for DIDO fuel elements

As an alternative solution to the DIDO insert described above, another variant is considered here for which the transport positions are out of boron steel rods. The rod wall thickness is 0.3 cm and the boron content of the steel is 0.6 weight percent. The internal diameter was retained (10.4 cm). Otherwise the conditions were the same as described in chapter 3.

Analogous with the illustration in chapter 3.2, group constants were calculated for the new basket lattice cells. The characteristic criticality values in table 10.1, corresponding to table 2, were collated from this calculation.

Table 10.1

% Vol.	R_{BE}	R_{H2O}	K_∞	B_m^2	τ	L^2
100	5.2	0.0	0.8973	-.00293	33.289	1.711
90	4.9332	0.2668	0.9090	-.00260	33.309	1.684
80	4.6510	0.5490	0.9063	-.00267	33.397	1.660
70	4.3506	0.8494	0.8899	-.00314	33.458	1.647
65	4.1924	1.0076	0.8765	-.00369	33.501	1.643
60	4.0279	1.1721	0.8594	-.00399	33.556	1.648
55	3.8564	1.3436	0.8386	-.00457	33.627	1.659
50	3.6770	1.5230	0.8136	-.00527	33.717	1.681
40	3.2888	1.9110	0.7496	-.00700	33.990	1.765

In comparison with table 2, it can be seen immediately from table 10.1 that the K_{∞}-values alone for all basket lattice cells are under 1. In addition, the container calculations indicated above, as well as the reactivity effects can be attributed in their order of magnitude to the present case. Consequently this boron steel basket can be considered as critically safe for the transport of DIDI fuel elements in the TN-7.

10.2 Boron steel basket for MERLIN fuel elements

The boron steel basket for the MERLIN fuel elements is once again formed of almost square steel boxes with an surface of 8.7 x 8.1 cm^2. These steel boxes differ from the non-poisoned insert boxes in so far as they have a wall thickness of 0.3 cm and a boron content of 0.6 %. For the rest the same conditions as in 4.2 prevail.

Analogous with figure 4, group constants for the cases illustrated in this figure were calculated. The characteristic criticality values are given in table 10.2.

Table 10.2

BE	6.3x3.76	6.3x7.52	7.56x7.96	7.96x7.96	8.7x8.1
K_{∞}	0.6686 (0.6544)	0.9514 (0.9359)	1.0003	1.0145	1.0184
M^2	42.960 (43.090)	39.784 (39.873)	39.534	39.412	39.335
B_m^2	-.0077 (-.0080)	-.0012 (-.0016)	$7.6 \cdot 10^{-6}$	.0004	.0005

When the values in table 10.2 are compared with those given in figure 4 it can be concluded that - on the one hand - the reactivity of the boron-poisoned lattice is much lower and that - on the other hand - the similar tendencies can be detected for the reactivity effects. As a result the multiplication factor for the TN-7 with an insert of these boron steel boxes will be much lower than inserts of unpoisoned steel as used in the experiments.

Appendix 8.2

Criticality safety of irradiated RHF fuel elements in the TN 7 transport flask

W. Weber, H. Krug, 27.4.1982

Criticality safety of irradiated RHF fuel elements in the TN 7 transport flask

W. Weber, H. Krug, 27.4.1982

1. PROBLEM DEFINITION

It is intended to transport 2 irradiated fuel elements from the high flux reactor in Grenoble (RHF fuel elements) in the TN 7 transport flask. For this purpose the transport flask must satisfy the requirements for the nuclear fissile class II, i.e. at least 2 flasks in a flooded, fully reflective state, and 5 flasks in a dry state are sufficiently sub-critical.

For transport, the RHF fuel elements will be sufficiently dis-assembled such that only the cylindrical active zone is transported (drawing no. Re 7C 65 R10, Institut Max von Laue - Paul Langevin). Both RHF fuel elements will be fixed in position inside the transport flask by means of a basket. Inside the transport flask itself there is also an additional shielding unit (drawing no. 1-150- 025-19-00, TN).

Although sub-criticality in the dry state can be proven by means of the available literature, a criticality analysis was necessary for the flooded state.

2. FLOODED FLASKS

2.1 Method of calculation

The multiplication factor for the flooded flasks was calculated using the Monte Carlo program KENO-IV (Lit. 1), with 15 fast and 1 thermal neutron groups. The effective cross-sections in P_1-approximation were produced using the GAMTEC program (Lit. 2), whereby for the fast groups a B_1-approximation and for the

thermal group with water moderation the Wigner-Wilkins approximation was used, in other cases a Maxwell spectrum at ambient temperature. In order to calculate the effective cross-sections of the fuel zone, the aluminium fuel plates were homogenised with water over the volume (formed from 6.19 cm annular gap between the aluminium load tubes and the active height of 80 cm). As a buckling constant, 10^{-4} was used.

2.2 Material data

Fuel isotopic composition:	9.2 kg U-235	ρ = 18.662 g cm^{-3}
(active zone)	17.086 kg Al	ρ = 2.698 g cm^{-3}
Steel composition:	DIN 1.4301	ρ = 7.566 g cm^{-3}
Densities:	Aluminium	ρ = 2.698 g cm^{-3}
	Lead	ρ = 10.77 g cm^{-3}
	Water	ρ = 1.00 g cm^{-3}

2.3 Geometrical model

In the calculation model, the ring-formed structure of the cross-section through the flask at the active zone level was reproduced in a lateral direction, whilst in the longitudinal direction a conservatively infinite length was assumed. Material zones and ring thicknesses (ΔR) are listed from inside to outside in the following table:

Zone	Material	ΔR (cm)	Component
1	water	11.20	
2	steel	0.80	basket
3	water	1.04	
4	aluminium	0.65	fuel element
5	fuel	6.19	fuel element
6	aluminium	0.80	fuel element
7	water	6.32	
8	steel	1.00	additional shielding
9	lead	5.20	additional shielding

10	steel	1.20	additional shielding
11	water	1.10	
12	steel	1.00	flask
13	lead	13.00	flask
14	insulation	3.00	flask
15	steel	2.00	flask

All empty spaces were, as you can see, completely filled with water. Instead of the insulation (zone 14) a vacuum was assumed, which in the present case is of minor importance for the criticality

For the Monte Carlo calculation, 2 flasks were represented touching side to side. In addition, these flasks were assumed to be surrounded by at least a 30 cm thick layer of water.

2.4 Result

The Monte Carlo calculation was programmed for 63 iterations, each with 300 neutrons, whereby the first 3 iterations were devoted to determining the multiplication factor. For the given sequence the result was:

$$K = 0.933 \pm 0.006 \qquad \text{(accurate to 1 } \sigma\text{)}$$

Thus, 2 touching flasks when fully flooded and water reflected are sufficiently sub-critical.

3. DRY FLASKS

There are no criticality problems for the flasks in a dry state. This can be shown by the following estimation. Assuming 9.2 kg U-235 and 17 kg aluminium for the fuel zone of an RHF fuel element, then in the fully compacted fuel mass the weight percent of U-235 is 35 % and the percentage volume of U-235 is 7.3 %. According to Lit. 3, Fig. 2.8, the critical though unreflected spherical mass at this concentration is about 1100 kg U-235.

The influence of a reflector can also be obtained by estimation (according to Lit. 3) by multiplying this unreflected mass by the relation of fully-concentrated reflected to unreflected spherical

masses. The experimental spherical masses of U(93) metal with no reflector is 49.3 kg (according to Lit. 4), and of U(93.5) metal with a 20 cm thick natural uranium reflector is 16.1 kg according to Lit. 5. Thus, the critical mass would be 359 kg.

The U-235 content of 5 transport flasks is 92 kg, which means that at least 5 transport flasks in a dry state are sufficiently sub-critical. The estimation carried out is very conservative, as the fuel zone is always assumed to be fully compacted. Bearing in mind the actual circumstances, it can be expected that even an infinite number of such flasks in a dry state are sub-critical, as detailled calculations with similar fuel have shown (see Lit. 6).

4. REFERENCES

/1/ L. M. Petrie et al.:
KENO-IV, An improved Monte Carlo criticality program
ORNL-4938, Nov. 1975

/2/ Carter, Richey, Hughey
GAMTEC-II, A code for generating consistent multigroup constants utilised in diffusion and transport theory calculations
BNWL-35, March 1965

/3/ H.K. Clark
Handbook of nuclear safety
DP-532, Jan. 61

/4/ J. H. Chalmers et al.:
Handbook of criticality data, vol. 1
1967

/5/ H. C. Paxton et al.:
Critical dimensions of systems containing ^{235}U, ^{239}Pu, ^{233}U
TID 7028, June 1964

/6/ H. Krug
Criticality safety of DIDO and MERLIN fuel elements in the TN 7
Dec. 1976

9. Quality assurance

9.1 Quality assurance manual

Quality assurance requirements are described in the TRANSNUKLEAR (TN) quality assurance manual /9-1/.

The contents of the manual are:

- Tasks and fields of application of the quality assurance system
- Organisation of the hierarchy and administration of TN including organisational charts, quality system and qualifications
- Purchasing in accordance with quality assurance requirements
- Quality assurance co-operation with suppliers
- Design and planning including development, calculations and design
- Inspection and revision of calculation, design, fabrication and testing documents as well as their release.
- Fabrication supervision and carrying out of tests and inspections
- Transport and storage
- Installation and commissioning
- Documentation including control and revision of documents
- Identification, archiving, traceability

The quality assurance manual applies to the areas of organisation, planning, fabrication, inspection and operation of the cask.

9.2 Fabrication and inspection

9.2.1 Generalities

The fabrication of the cask from its components is carried out in accordance with fabrication follow-up plans (FPP) determined by TN and the manufacturer and approved of by independent experts prior to the start of fabrication.

The manufacturer records the individual fabrication and inspection steps.

The independent expert and/or TN will inspect the progress of fabrication and the results of tests carried out at predetermined intervals.

The manufacturer follows up fabrication and inspection documentation and submits it to TN for inclusion in the.overall documentation following comple-tion of the individual cask components after approval by the independent ex-pert, TN and the manufacturer.

9.2.2 Selection of manufacturer

Prior to the placing of an order, TN will investigate whether the manufactu-rers invited to tender fulfil the following quality assurance requirements:

- Organisational structure of the manufacturer
  - Organisational charts and structuring
  - Quality assurance system
    - Independent quality assurance department (with direct access to company management)
  - A quality assurance department independent of manufacturing
  - Control of quality assurance measures
    - Control of drawings/parts lists, inspection plans, welding plans
    - Material deliveries

- Welding supervision
- Inspection supervision
- Stamp control and re-stamping
- Gauging

- Licences in accordance with technical regulations
- Staff qualifications

- Determination of the quality assurance system
  - Availability of one or more quality assurance manuals
  - Availability of a quality assurance program or quality assurance specifications

- Testing and inspection prior to the start of fabrication
  - Examination of the fabrication sites, machines and products as regards cleanliness
  - Verification that all employed welders have valid professional certifications
  - Proof of valid process inspections in accordance with AD specifications
  - Materials
    - Material reception examinations
    - Identification and marking examination (stamping)
    - Assignability of the material records
    - Inspection and archiving of material records
    - Storage of semifinished materials and welding additives

- Testing and inspection during fabrication
  - Recording of fabrication and inspection steps
  - Carrying out of intermediary inspections in accordance with written instructions
  - Deviations as regards inspection methods and their recording
  - Nonconformances in relation to fabrication methods and their recording
  - Carrying out and recording of repair measures

- Welding controls
  - Control by the welding supervisor
  - Presentation of valid welding certificates
  - Examination of the welding data in relation to the welding plan
  - Comparison of welding additives (inspection as to confusions)
  - Examination and validity of welding methods
  - Examination of weld seam preparations
  - Carrying out and recording of repairs and corrections
  - Storage of welding additives

- Inspection of synthetic materials in accordance with specifications

- Inspection of the coat of paint in accordance with TN specifications

- Testing and inspections
  - Carrying out and recording of non-destructive testing
  - Carrying out of destructive testing
  - Storage, inspections and adjusting of testing equipment

- Documentation
  - Inspection of the documentation department
  - Organisation of documentation according to TN specifications
  - Archiving documentation

When a manufacturer is invited to tender, he is previously provided the TN order specifications and draft drawings of the cask. The final specifications will be worked out by TN in collaboration with the manufacturer, based on the order specifications.

9.2.3 TN specification TN 7-2

The specification contains the following main items:

- field of application and responsibilities
- specification changes
- design characteristics of the cask
- cask description
- handling description
- classification of components according to requirement categories
- description and specification of components
- material specifications
- submission of preliminary inspection documents
- taking into account of technical regulations and TN regulations
- materials testing
- carrying out of welds
- testing and inspection during fabrication
- testing and inspection of the finished cask (final acceptance)
- documentation
- fabrication inspection plan
- material data sheets
- fabrication follow-up plan
- inspection plans
- drawings

Specification "TN 7-2 Transport Cask for Spent Fuel Assemblies", no. 06 BBO 23 revision 3 /9-2/ thus prescribes the entire fabrication process. Prior to fabrication, the documents are submitted to the competent authorities for preliminary inspection and fabrication clearance.

9.2.4 Preliminary inspection documents

Preliminary inspection documents are:

- TN 7-2 specification
- materials data sheets
- fabrication follow-up plan
- welding plan
- fabrication blueprints and parts lists
- welding blueprints

Fabrication of the components will only begin after clearance of the preliminary inspection documents has been granted by the competent authority.

9.2.4.1 Specification TN 7-2

Cf. chapter 9.2.3

9.2.4.2 Construction materials data sheets

The material data sheets list all the materials and standard parts used for the fabrication of the cask, corresponding data and the inspections to be carried out. Depending on the grading of the individual component the scope of inspections and the type of required verifications is determined. Material data sheets are examined by the competent authority. They are part of the specifications. Materials are selected on the base of generally accepted technical regulations.

9.2.4.3 Fabrication follow-up plan

The fabrication follow-up plan indicates inspections required prior to, during and following fabrication, based on the fabrication inspection plan. The main fabrication and inspection steps pertaining to the fabrication of the individual components are described chronologically. Implementation is confirmed, depending on the specification grading, by the manufacturer, TN and/or an independent expert.

The fabrication follow-up plan also contains references with regard to the documents it is based on, fabrication regulations to be complied with and inspection regulations.

9.2.4.4 Welding plan

The welding plan is worked out in accordance with TN specifications. It contains following information (if required):

- welding plan number
- order number
- purchaser
- subject
- number of blueprint
- designation of the welding materials
- welding method
- work samples
- preheating temperature/temperature of intermediate layers
- electrode drying
- welding data
- weld seam inspections
- sketches with running weld numbers
- weld seam preparation
- treatment of edges

- root face finishing
- weld seam sequence
- number of layers
- weld seam finishing
- acceptance

The welding plan must be cleared by the competent authority before fabrication may begin. Its requirements must be complied with.

9.2.4.5 Fabrication and welding blueprint

If necessary, fabrication and welding blueprints for all components will be submitted for preliminary inspection. In this case, fabrication blueprints also include welding blueprints with every weld seam marked in accordance with the numbering in the welding plan.

Fabrication blueprints include the corresponding parts lists.

9.2.4.6 Changes of the quality assurance plan

The quality assurance plan includes all preliminary inspection documents. It also includes specific work and inspection instructions.

Any change of the quality assurance plan resulting from preliminary inspection will cause the implementation of the following measures, depending on the requirement category:

- For parts which fall by definition into requirement category I, changes will be reported by the manufacturer to TN, to the officially approved expert and to the competent authority. Any deviation will require the approval of the authority.

- For parts falling under requirement category II, TN and the independent expert shall be informed. Any alteration or deviation requires the latter's approval.

- For parts falling under requirement category III, TN is informed. TN's approval is required for any alteration. The official expert is informed about the alteration.

9.2.5 Special working and inspection instructions

Special working and inspection instructions are worked out by TN for some fabrication steps, or in collaboration with the manufacturer.

This particularly concerns insertion of the thermal insulation (cement). The manufacturer will investigate the behaviour of the cement during and after casting in the course of preliminary tests. The casting of cement into the 1/3 scale model, following simulation tests, will serve as a process qualification for the casting of cement into the original TN 7-2 cask.

Similarly, the painting of the outer cask surface is carried out according to TN working instructions, except for the trunnions. Requirements concerning the paint are listed in the TN specifications.

9.2.6 Destructive and non-destructive tests

The different cask components will continuously be submitted to tests during fabrication.

Where this is considered necessary, process and accompanying samples will be submitted to destructive tests. Non-destructive tests, such as ultrasonic tests, surface crack testing, gauging etc. will be carried out during fabrication.

For every component there is a material data sheet which indicates:

- the type of inspection
- the extent of testing
- verification
- tester

During fabrication, the components will be submitted to additional non-destructive tests. These tests are defined in the fabrication and test follow-up plans.

9.2.7 Acceptance

After completion and assembly of the cask, the following tests are carried out in accordance with the fabrication follow-up plan, in the presence of the appointed independent expert, of the manufacturer and of TN. Correct execution of these tests is confirmed by the independent expert:

- stamp control
- examination of the confirmed fabrication and inspection follow-up plan
- leak tests
- load tests of the handling components followed by tests of their weld seams
- gauging
- examination of documentation

The manufacturer will carry out inspections and handling tests in presence of TN. These will demonstrate that the cask and its handling components can be handled without problem. These tests comprise:

- determination of weight
- examination of the surface as to absence of ferrite

- pressure test and visual inspection of the containment
- heating test
- examination of the coat of paint
- examination of the cask markings according to TN specifications
- handling tests:
  . installation and disassembly of all lids and connections
  . attachment and removal of the trunnions
  . turning of the cask over the lower pair of trunnions
  . testing of the proper function of the cask openings
  . vacuum drying

Following the tests to be supervised by the independent expert, the cask will be stamped for release if there are no objections, and marked with the date of the next periodic inspection.

9.3 Integrated fixtures

A. Insert baskets for DIDO and MERLIN fuel assemblies

The insert baskets for DIDO and MERLIN fuel assemblies are welded stainless steel structures (cf. chapter 3)

The same insert baskets are used in the TN 7-2 cask as in the TN 7.

Additionally, a new insert basket for MERLIN fuel assemblies will be built based on the existing MERLIN basket. This new basket will be fabricated observing the usual quality assurance requirements in accordance with TN
specifications as well as fabrication and inspection follow-up plans.

B. RHF basket

The RHF basket (cf. chapter 3) is a welded stainless steel structure.

The basket will be fabricated in accordance with TN specifications and fabrication and inspection follow-up plans, observing quality assurance requirements.

9.4 TN 7-2 transport cask - 1/3 scale model

The cask model is fabricated by the same manufacturer as the original cask. Fabrication and inspection of the model are carried out in accordance with TN specifications /9-3/. These specifications are submitted for preliminary inspection together with the fabrication and welding blueprints and a welding plan. Any changes to these documents are also subject to approval as set out in chapter 9.2.4.6.

The scope of tests during the fabrication of the model is smaller than that required for the original cask; however, it will be ensured that the 1/3 scale model is representative of the original cask during tests. This will, in particular, mean that dimension relations of the model are according to the same scale, that the same or at least comparable materials are used and that the welds are comparable. For this purpose, material verifications are carried out, if possible by means of 3.1 B certificates, and a welding plan is drawn up.

Deviations occurring in the scale model are such that they either have no consequence or are conservative as far as the drop and fire tests are concerned.

9.5 Literature

/9-1/ TN Quality Assurance Manual, Revision 0
February 1982

/9-2/ Specifications for the TN 7-2 Transport Cask for Irradiated Fuel Assemblies, no. 06 BBO 23 Revision 4

/9-3/ Specifications for the 1/3 Scale Model of the TN 7-2 Transport Cask for Irradiated Fuel Assemblies no. 06 BBO 24 Revision 2

10. Handling and periodic inspections

The main handling steps with regard to the loading and unloading of the cask are described below inasmuch as they are safety relevant (cf. Fig. 10-1). The description will cover the various types of loading in common without taking into account differing local conditions. In addition, detailed handling instructions will be worked out for the various types of loading.

Should the cask be handled in other nuclear facilities, this will be considered in new instructions if necessary.

Carrying out of tests by the operator prior to each loading are part of the handling instructions. Periodic inspections are those tests carried out at certain time intervals, some of them in the presence of an independent expert.

10.1 Loading of cask

10.1.1 Preparations for loading

- Visual inspection of the overall condition, if necessary cleaning of the cask.
- Taking of a gas sample from the inside and analysis (only in the case of RHF fuel).
- Leak check in accordance with TN specifications prior to loading (if any leakage is discovered, the gaskets are replaced and the tests are repeated).
- Unscrewing of the cask lid screws and screwing-in of the eyebolts.
- Removal of the coupling in the cask bottom (position A) and attachment of the matching coupling in the lid (position B).

- Placing the lid centring pins in two lid screw holes.
- Removal of cask lid (in the case of RHF fuel, this operation, together with the following activities, is not carried out under water; normally this is carried out in the pond).
- Visual inspection of the lid and the cask cavity.
- Removal of the insert baskets from the cask, visual inspection of the cask cavity (particular care should be taken that no components are lying around in the cask).
- Visual inspection of the insert baskets, if necessary, a test loading with a dummy will be carried out.

10.1.2 Loading

- The cask is set down in the pond with the help of a crane. The crane attachments are removed from the cask (this will normally be done prior to the removal of the cask lid).
- The fuel assemblies are loaded into the insert baskets.
- The loaded baskets and the spacers are placed inside the cask.
- The lid is attached under water, taking particular care taken as to proper fitting.
- The cask is lifted up to the water surface and the lid is provisionally secured with three screws.
- The cask is lifted altogether out of the water and rinsed on the outside with fully demineralized water. While the cask is lifted out, the dose rate is being monitored.
- The cask is emptied of water above the pond and then placed in its predetermined position.
- Coupling A is screwed in.

10.1.3 Preparation for transport

- The lid centring bolts are unscrewed.
- The lid screws are applied and fastened with a torque of 400 Nm.
- The cask cavity is dried (vacuum drying over the bottom connection (A), with lid connection (B) closed. For this, the cavity must be evacuated to less than 20 Torr.
- Transport vacuum of 0.6 bar is adjusted.
- The drying equipment is removed and the protective lid applied over the couplings (A, B). Tightening torque of the screws: 15 Nm.
- Leak checks are carried out in accordance with TN specifications. A leak rate of $L \cong 1 \cdot 10^{-2}$ is determined for the cask. This is demonstrated by loss of pressure.
- The testing connections are closed off and the cask is sealed.
- The shock absorbers are fitted.
- The cask is decontaminated. According to traffic regulations, the maximum admissible values are:

$$\alpha : 10^{-5}\ \mu Ci/cm^2$$
$$\beta + \gamma : 10^{-4}\ \mu Ci/cm^2$$

- The cask is inspected for compliance with the traffic regulations concerning dose rate, surface temperature and contamination.

10.2 Unloading of cask

10.2.1 Preparations for unloading

- Receiving inspection of the cask:
  dose rate, temperature and contamination are checked, the overall condition of the cask is examined.
- The shock absorbers are removed.
- The protective lid covering the coupling (positions A and B) is removed.
- A gas sample is taken at connection A.
- The coupling is removed from connection A.
- Lid coupling (B) is connected to a hose which is closed off at the end.
- The cask is lowered into the pond and left to cool down (about 4 hours).
- Water is let through the lower opening into the cask by opening up the hose. The end of the hose is held under water in order to allow released steam to condense. The filling of the cask will take approximately one hour.

10.2.2 Unloading

- The cask is lifted up to the water surface, the lid screws are unfastened and the centring bolts are screwed in.
- The cask is lowered again.
- The cask lid is drawn under water.
- The baskets containing the fuel assemblies are unloaded from the cask.
- The empty baskets are reloaded.
- The cask is lifted from the pond and rinsed on the outside with fully demineralized water.
- The cask is emptied of water over the pond and then placed in a predetermined position.

10.2.3 Preparations for transport

- The lid is applied, centring bolts are removed and screws are fastened.
- The lower coupling (A) is screwed in.
- The cask cavity is dried (vacuum drying).
- The protective lid is placed over the couplings.
- The cask is decontaminated.
- The shock absorbers are fitted.
- The cask is inspected for compliance with the traffic regulations concerning dose rate, surface temperature and contamination.

10.3 Periodic inspections

The plan for periodic inspections is contained in appendix 10.1.

Appendix 10.1

Plan for periodic inspections

Plan for periodic inspections of the TN 7-2 transport cask

These inspections are carried out by the officially approved expert. The inspection interval is set at four years.

The following inspections will have to be carried out:

1. External and internal visual inspection of the overall condition as regards corrosion and mechanical changes.

2. Visual examination of the gasket surfaces with regard to corrosion and mechanical damages.

3. Visual examination of the screws for mechanical damage.

4. Inspection of the type plate as to completeness.

5. Visual examination of the fuel assembly insert baskets with regard to corrosion and mechanical changes.

6. Surface crack inspection of the trunnions as well as of the weld seams marked in Fig. 10-1 using the dye penetration process. This is carried out and evaluated in accordance with TN inspection procedure no. 04-100-1981.

7. Leak checks of the lid gasket and the two coupling lids.
   Maximum total leak rate for the cask: 10^{-4} Torr · l/sec

   Inspection space between the double gaskets: maximum leak rate
   $3 \cdot 10^{-4}$ Torr · l/sec

The tests are carried out using a process which ensures that the leak rates quoted above can be detected. This may be for example helium leak test or tests of pressure increase test or drop of pressure.

11. Drawings

The following drawings are joined to the safety report. They are referred to in the text:

• Overview	No. 0-150-050-04-00
• Cask body	No. 0-150-050-05-00
• Cask lid	No. 0-150-050-06-00
• Lid shock absorber	No. 1-150-050-07-00
• Bottom shock absorber	No. 1-150-050-08-00
• Type plate	No. 3-150-050-03-00
• Insert baskets for MERLIN and DIDO fuel assemblies	No. 1-150-025-17-00
• Insert basket for 2 RHF fuel assemblies	No. 1-150-025-21-00

Appendix 8.1

Criticality safety of DIDO and MERLIN fuel assemblies in the TN 7 cask

(H. Krug, Technische Universität München,
December 1976)

TN	Plan for Periodic Inspections	Page 2 of 2

Ref.: TN 7-2 Drawing no: 0-150-050-04-00

Explanations:

TN - TRANSNUKLEAR

T - officially approved expert

Part 2:

Test after 4 years

No	Description of inspection	Inspection procedure	Inspector	
	step		TN	T
1	Inspections according to Part 1, no. 1, 2 and 5		x	
2	Exterior and interior inspection of overall conditions for corrosion and mechanical changes	visual		x
3	Inspection of gasket surfaces for corrosion and mechanical changes	visual, rework if necessary		x
4	Surface crack inspection of lid and protective lid screws	TN inspection procedure no. 04-100-1981		x
5	Control of all threads as to easy going	Working procedure, rework if necessary		x
6	Removal of trunnions, surface crack inspection of parts which are not accessible from outside, surface crack inspection of trunnion screws	TN inspection procedure no. 04-100-1981		x
7	Check of trunnion load with 125 % load, followed by surface crack inspection	TN inspection procedure Working procedure no. 04-100-1981		x
8	Surface crack inspection of the weld seams of the trunnion holders and the connecting seams of the exterior mantle with the bottom and the covering plate	TN inspection procedure no. 04-100-1981		x
9	Inspection of the insert baskets or corrosion and mechanical changes	visual		x
10	Inspection of the cask cavity for corrosion and mechanical changes	visual	x	
11	Helium leak check at gaskets of lid and protective lid	TN inspection procedure no. 04-110-1982		x
12	Inspection of shock absorbers for tightness	TN inspection procedure, gas pressure 1.1 bar, soap bubble test	x	

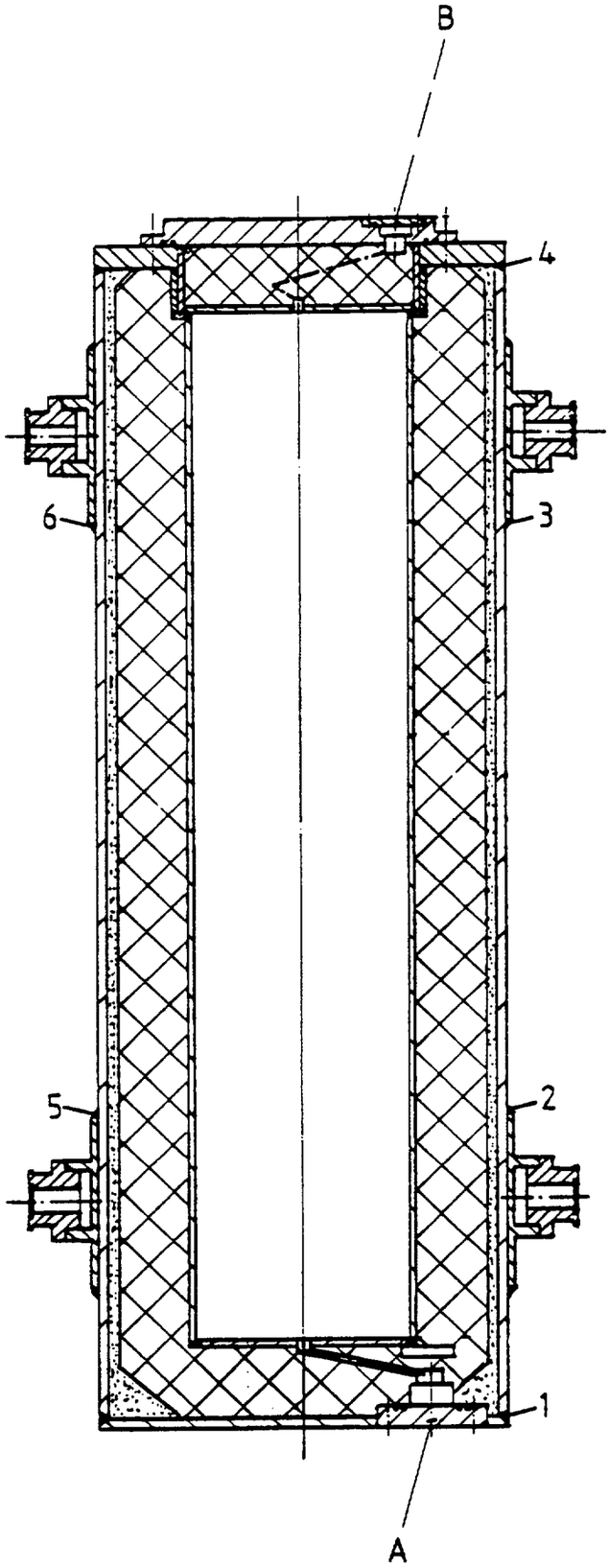

(1 - 6 subject to periodic inspections)

TN	Transport cask TN 7-2	Fig. 10-1